Table 3
Summary of cases of tumor seeding

No.	Age	Sex	Size (mm)	Location	Distance from pleura (mm)	Co-axial method	No. of biopsy	Technique of biopsy	Size of the needle
1	72	M	30	Right upper	0	No	1	Core biopsy	18G
2	73	M	30	Left lower	30	Yes	3	Core biopsy	18G
3	71	M	10	Right upper	20	No	2	Aspiration biopsy	22G
4	30	F	28	Left upper	76	No	2	Core biopsy	18G
5	69	M	15	Right lower	0	No	2	Core biopsy	21G
6	77	M	12	Right upper	30	Yes	2	Core biopsy	20G

rate of 0.06%, which also shows no major difference from the previously reported complication rate. However, in the present study, there were several cases of severe complications including cardiac and respiratory arrest, and shock, which can be secondary to air embolism, although it is very difficult to confirm air embolism in the coronary artery in cases of myocardial infarction when the patient has not been scanned at the level of the heart. It is speculated that concurrent cough during the procedure has a high possibility of an air embolism misplacing the biopsy needle into the large vessel adjacent to the pulmonary lesion. Among the total of six cases with air emboli in the present study, two cases demonstrated biopsied pulmonary lesions located close to the large vessels, however the remaining four cases have no close relation to the large vessels. There were no reports of coughing during the procedure in any of the cases complicated by air embolism. Air embolism even occurred in a case in which the nodule was very near the pleura (case no. 5). In our study, all cases with air emboli had undergone CT-guided biopsy using a core biopsy needle of 18–20 gauge, which is greater in diameter than the usually used fine aspiration needles. Having said that, in the previous reviews, most cases with air emboli were biopsied by fine aspiration needles, and there are two prior reports of air embolism following CT-guided lung needle marking using thin needles without recent biopsy [24–26].

Tumor seeding into the needle tract seems to be a rare possibility in several case reports [27–34]. There were six cases (0.06%) of tumor seeding in our study, which is a relatively high frequency compared to previous studies [5,35]. The true incidence of tumor seeding along the needle may be underestimated as not all cases can be diagnosed, and many patients die before these metastases become clinically apparent. Tumor seeding appears to depend on the size of the needle, therefore large-bore needles carry a relatively greater risk of tumor seeding, however tumor seeding following a fine needle aspiration was reported in one case of our study. It is thought that CT-guided biopsy performed using the Co-axial method has less frequency of tumor seeding as the outer cannula minimizes direct contact of the tumor cells with the biopsy route. Surprisingly, tumor seeding occurred in two cases using the Co-axial method. We speculate that the outer cannula was not appropriately placed.

Unfortunately, there were seven patients (0.07%) who died in our study due to complications in the CT-guided needle biopsy. Greene [6] estimated the mortality rate associated with fine needle aspiration to be 0.02%, however Richardson et al. [8] reported eight deaths (0.15%) in their study due to complications in CT-guided needle biopsy. Most of the deaths in the present study were attributed to fatal air embolism. Three cases of air embolism that were treated with hyperbaric oxygen recompression were recovered without sequela, which may suggest hyperbaric oxygen recompression therapy is effective for treatment of air embolism, and for reducing the mortality rate.

Our study has several limitations, including selection bias, the long period of the study, multi-center analysis with a large variety of techniques and CT scanners, and the possibility of missing or misdiagnosing significant complications such as the number of air emboli and tumor seeding. Moreover, our study is a retrospective questionnaire-based analysis rather than a prospective survey.

In conclusion, this is the first nation-wide study documenting severe complications with respect to CT-guided needle biopsy in Japan. The complication rate in Japan is comparable to internationally published figures. We believe this data will improve both clinicians as well as patients understanding of the risk versus benefit of CT-guided needle biopsy, resulting better decisions.

Acknowledgement

The authors, members of the Japanese lung biopsy conference, dedicate this manuscript to Dr. Junpei Ikezoe, originator of this conference. We are also grateful to those specialists who completed the questionnaire. The authors thank Dr. Javzandulam Natsag for his assistance with manuscript editing.

References

[1] Sinner WN. Pulmonary neoplasms diagnosed with transthoracic needle biopsy. Cancer 1979;43:1533–40.
[2] Klein JS, Zarka MA. Transthoracic needle biopsy. J Thorac Imag 1997;12:232–49.
[3] Hirose T, Mori K, Machida S, et al. Computed tomographic fluoroscopy-guided transthoracic needle biopsy for diagnosis of pulmonary nodules. Jpn J Clin Oncol 2000;30:259–62.
[4] Berquist TH, Bailey PB, Cortese DA, et al. Transthoracic needle biopsy: accuracy and complication in relation to location and type of lesion. Mayo Clin Proc 1980;55:475–81.
[5] Sinner WN. Complications of percutaneous transthoracic needle aspiration biopsy. Acta Radiol Diag 1976;17:813–28.

[6] Greene RE. Transthoracic needle aspiration biopsy. In: Athanasoulis CA, Pfister RC, Greene RE, Robertson GH, editors. Interventional radiology. Pliladelphia: Sanders; 1982. p. 587–634.
[7] Klein JS, Zarka MA. Transthoracic needle biopsy. Radiol Clin North Am 2000;38:235–66.
[8] Richardson CM, Pointon KS, Manhire AR, et al. Percutaneous lung biopsies: a survey of UK practice based on 5444 biopsies. Br J Radiol 2002;75:731–5.
[9] Belfiore G, Filippo SD, Guida C, et al. CT-guided needle biopsy of lesions. Nucle Med Biol 1994;21:713–9.
[10] Wescott JL. Air embolism complicating percutaneous needle biopsy of the lung. Chest 1973;63. pp. 108–108.
[11] Aberle DR, Gamsu G, Golden JA. Fatal systemic arterial air embolism following lung needle aspiration. Radiology 1987;165:351–3.
[12] Cianci P, Posin JP, Shimshak RR, et al. Air embolism complicating percutaneous thin needle biopsy of lung. Chest 1987;92:749–50.
[13] Tolly TL, Feldmeier JE, Czarnecki D. Air embolism complicating percutaneous lung biopsy. AJR Am J Roentgenol 1988;150:555–6.
[14] Baker BK, Awwad EE. Computed tomography of fatal cerebral air embolism following percutaneous aspiration biopsy of the lung. JCAT 1988;12:1082–3.
[15] Worth ER, Burton RJ, Landreneau RJ, Eggers GWN, et al. Left atrial air embolism during intraoperative needle biopsy of a deep pulmonary lesion. Anesthesiology 1990;73:342–5.
[16] Wong RS, Ketai L, Temes RT, Follis FM, et al. Air embolus complicating transthoracic percutaneous needle biopsy. Ann Thorac Surg 1995;59:1010–1.
[17] Khatri S. Cerebral artery gas embolism (CAGE) following fine needle aspiration biopsy of the lung. Aust NZ J Med 1997;27. pp. 27–27.
[18] Regge D, Gallo T, Galli J, et al. Systemic arterial air embolism and tension pneumothorax: two complications of transthoracic percutaneous thin-needle biopsy in the same patient. Eur Radiol 1997;7:173–5.
[19] Kodama F, Ogawa T, Hashimoto M, et al. Fatal air embolism as a complication of CT-guided needle biopsy of the lung. JCAT 1999;23:949–51.
[20] Shetty PG, Fatterpekar GM, Manohar S, et al. Fat cerebral air embolism as a complication of transbronchoscopic lung biopsy: a case report. Aust Radiol 2001;45:215–7.
[21] Arnold BW, Zwiebel WJ. Percutaneous transthoracic needle biopsy complicated by air embolism. AJR Am J Roentgenol 2002;178:1400–2.
[22] Mokhlesi B, Ansaarie I, Bazen B, et al. Coronary artery air embolism complicating a CT-guided transthoracic needle biopsy of the lung. Chest 2002;121:993–6.
[23] Laurent F, Montaudon M, Latrabe V, et al. Percutaneous biopsy in lung cancer. Eur J Radiol 2003;45:60–8.
[24] Ohi S, Ito Y, Keiya H, et al. Air embolism following computed tomography-guided lung needle marking; report of a case. Kyobu-Geka 2004;57:421–3.
[25] Kamiyoshihara M, Sakata K, Ishikawa S, et al. Cerebral arterial air embolism following CT-guided lung needle marking; report of a case. J Cardiovasc Surg 2001;42:699–700.
[26] Sakiyama S, Kondo K, Matsuoka H, et al. Fatal air embolism during computed tomography-guided pulmonary marking with a hook-type maker. J Thorac Cardiovasc Surg 2003;126:1207–9.
[27] Muller NL, Bergin CJ, Miller RR, et al. Seeding of malignant cells into the needle track after lung and pleural biopsy. J Can Assoc Radiol 1986;37:192–4.
[28] Redwood N, Beggs D, Morgan WE. Dissemination of tumor cells from fine needle biopsy. Thorax 1989;44:826–7.
[29] Berger RL, Dargan EL, Huang BL, et al. Dissemination of cancer cells by needle biopsy of the lung. J Thor Cardiovasc Surg 1972;63:430–2.
[30] Freise G, Larios R, Takeno Y, et al. Cell dissemination and implantation of neoplasms through biopsy and excision of malignant tumors. Dis Chest 1967;52:485–9.
[31] Christensen ES. Iatrogenic dissemination of tumor cells. Dissemination of tumour cells along the needle track after percutaneous, transthoracic lung biopsy. Danish Med Bull 1978;25:82–7.
[32] Ferrucci JT, Wittenberg J, Margolies MN, et al. Malignant seeding of the tract after thin-needle aspiration biopsy. Radiology 1979;130:345–6.
[33] Yoshikawa T, Yoshida J, Nishimura M, et al. Lung cancer implantation in the chest wall following percutaneous fine needle aspiration biopsy. Jpn J Clin Oncol 2000;30:450–2.
[34] Kara M, Alver G, Sak SD, Kavukcu S. Implantation metastasis caused by fine needle aspiration biopsy following curative resection of stage IB non-small cell lung cancer. Eur J Cardiothor Surg 2001;20:868–70.
[35] Ayar D, Golla B, Lee JY, Nath H. Needle-track metastasis after transthoracic needle biopsy. J Thorac Imag 1998;13:2–6.

Consistent Liver Metastases in a Rat Model by Portal Injection of Microencapsulated Cancer Cells

Tsuyoshi Enomoto,[1] Tatsuya Oda,[1] Yasuyuki Aoyagi,[1] Shinji Sugiura,[3] Mitsutoshi Nakajima,[4] Mitsuo Satake,[5] Masayuki Noguchi,[2] and Nobuhiro Ohkohchi[1]

Departments of [1]Surgery (Graduated School of Comprehensive Human Science) and [2]Pathology, Institute of Basic Medicine, University of Tsukuba; [3]Research Center of Advanced Bionics, National Institute of Advanced Industrial Science and Technology; [4]Food Engineering Division, National Food Research Institute, Tsukuba, Ibaraki, Japan; and [5]Radiology Division, National Cancer Center Hospital East, Kashiwa, Chiba, Japan

Abstract

Consistent liver metastases in animal models is generally observed only with certain cancer cell lines. With the aim of improving on existing animal models of liver metastases, we hypothesized that cancer cells encased in 300 μm microcapsules, mimicking micrometastatic foci, might be effective seeds of liver metastases. A total of 3,000 microcapsules, containing 700 to 1,500 viable cells/capsule in logarithmic growth phase of three human pancreatic cancer cell lines (SUIT-2, AsPC-1, and BxPC-3), were transplanted in nude rats by portal injection. The rate of liver metastases was 100% (12 of 12), 100% (6 of 6), and 83% (5 of 6) for SUIT-2, AsPC-1, and BxPC-3 microcapsules, respectively. In contrast, the administration of an identical number of single cancer cells (2.1–4.5 × 10^6) did not lead to liver metastases. Metastases was strictly limited to the liver, was quite stable, and could be proportionately tailored by varying the number of cancer microcapsules administered. Microscopic observation showed that two-thirds of the cancer microcapsules were lodged in the peripheral small (20–50 μm) portal veins, although one-third of the cancer microcapsules were trapped in the central wide (200–400 μm) portal vein. Capsules began to burst at day 3, with recognizable metastases produced at day 7, resulting in overt metastases production at days 28 to 42. The present cancer microcapsule method may be useful for obtaining liver metastases in animal models, especially for cell lines that will not form liver metastases with conventional single cell injection methods and/or for experiments requiring the consistent formation of liver metastases. (Cancer Res 2006; 66(23): 11131-9)

Introduction

Liver metastases is one of the most common forms of hematogenous spread in patients with various malignancies (1, 2), and the development of effective treatment modalities for liver metastases using convenient animal models is highly desirable. Because the liver is the largest solid organ, a reliable animal model of liver tumors is also valuable for *in vivo* evaluation of various therapeutic agents. However, representation of liver metastasis in an animal model using conventional approaches has proved difficult.

One commonly used approach for obtaining liver metastases is by injecting cancer cell suspensions into the hepatic portal veins or the spleen (3). However, liver metastases are consistently generated only with certain cell lines of the pancreas, colon, and stomach that have a high metastatic potential to liver (4–8). Moreover, many cell lines do not generate consistent liver metastases when administered as single cell suspensions (7–9). An additional obstacle with this model is that tumor growth occurs in sites other than the liver, such as the injected spleen and/or peritoneum (10). In fact, these undesirable tumor growths make experiments focusing on liver metastases difficult to interpret and largely inhibit the appearance of liver metastases (11, 12). Alternative strategies for obtaining liver metastases with cancer cells of low metastatic potential include orthotopic implantation, by injecting cancer cell suspensions, or by surgical transplantation of tumor fragments (13–15). Obstacles in the latter strategy include the presence of undesired metastases and are moreover difficult to reproduce in terms of the frequency and extent of metastases (16–18).

The formation of hematogenous metastases has been explained by two major theories, i.e., the seed and soil hypothesis by Paget (19) and the anatomic mechanical trapping theory of Ewing (20). The former suggests that metastases occurs only when the metastatic capacity of certain cancer cells (= seed) and environments of target organs (= soil) are compatible. The latter theory proposes that the anatomic location of the primary tumor and target organs, i.e., nonspecific trapping of cancer cells in the microvasculature, plays an important role in the development of metastases. Both mechanisms may also jointly contribute to the development of liver metastases in a clinical setting. The fact that even pancreatic cancer cell lines, which are clinically notorious for frequent presentation of liver metastases, do not consistently present liver metastases in animals (7, 8) forces the consideration that one of the difficulties in developing liver metastases in an animal model may be that the mechanical trapping process is not adequately reproduced.

With the aim of improving on existing animal models of liver metastases, we hypothesized that mechanical trapping could be rendered more efficient by aggregating multiple cancer cells. For this purpose, we employed cell encapsulation technology, previously used for pancreatic islet cell transplantation (21), which enabled us to consistently encase cancer cells into uniform 300 to 700 μm capsules. The preincubation of cancer cell containing cancer microcapsules *ex vivo* could substitute the initial proliferation step of cells, effectively providing cells in the logarithmic growth phase. When these cancer microcapsules are injected in the portal vein, they may become physically trapped in the peripheral vasculature of the liver before bursting and could thus act as seeds of liver metastases.

Note: Y. Aoyagi is a recipient of a Postdoctoral Fellowship from the Japan Society for the Promotion of Science, Tokyo, Japan.

Requests for reprints: Tatsuya Oda, Department of Surgery, Institute of Clinical Medicine, University of Tsukuba, 1-1-1 Tennondai, Tsukuba, Ibaraki 305-8575, Japan. Phone: 81-298-53-3221; Fax: 81-298-53-3222; E-mail: tatoda@md.tsukuba.ac.jp.

doi:10.1158/0008-5472.CAN-06-0339

Herein, we report a novel utilization of cancer cell microencapsulation that acts as an effective seed of liver metastasis in a rat model. Transplantation of *ex vivo* precultured 300 μm cancer microcapsules, formed from three different human pancreatic cancer cells, into the liver of nude rats via a portal vein resulted in efficient and stabile production of liver metastases.

Materials and Methods

Cell Lines

Three human pancreatic cancer cell lines (SUIT-2, AsPC-1, and BxPC-3) were used. SUIT-2 cells were generously provided by Dr. Iwamura (Miyazaki Medical College, Miyazaki, Japan; ref. 22), AsPC-1 and BxPC-3 were obtained from the American Type Culture Collection (Bethesda, MD). SUIT-2 was maintained in DMEM (Sigma-Aldrich, Taufkirchen, Germany) containing 5% fetal bovine serum (Sigma-Aldrich). AsPC-1 and BxPC-3 cultured in RPMI 1640 (Sigma-Aldrich) supplemented with 10% fetal bovine serum.

Cancer Cell Encapsulation to Form Artificial Cancer Cell Aggregates

Cancer microcapsules were engineered by conventional coaxial airflow methods (23). The size of the cancer microcapsules was targeted to ~300 μm because capsule sizes >100 μm were assumed to be beneficial for physical trapping in the peripheral portal vein in the liver, whereas those <300 μm are technically difficult to produce.

SUIT-2 cancer cell pellets were suspended in a 1.5% solution of potassium alginate (Kimica Corp., Tokyo, Japan) and the density was adjusted to ~1×10^7 cells/mL. AsPC-1 and BxPC-3 cancer cell pellets were encapsulated in the same manner, except that Matrigel (BD Biosciences, Bedford, MA) in a 25% (vol/vol) was added and the cell density was increased to ~2×10^7 cells/mL, because the proliferation of these cell lines was slow in pure alginate alone. The cell-alginate mixture was extruded through a 31-gauge needle at 5.0 mL/min and sheared by airflow, resulting in the formation of droplets having a diameter of 300 μm. The alginate droplets were allowed to directly fall into a cationic solution of 1.1% $CaCl_2$, promoting gel formation. The calcium alginate beads were chemically cross-linked with 0.05% (wt/vol) poly-L-lysine in 0.9% NaCl for 3 minutes. The capsules were recoated with 0.03% (wt/vol) alginate in 0.9% NaCl for 4 minutes. Finally, the remaining alginate core was dissolved with 1.6% (wt/vol) sodium citrate for 6 minutes.

In vitro Culture of Cancer Microcapsules: Capsule Burst, Histology and Cell Proliferation

Cancer microcapsules were incubated *in vitro* for several days at 37°C in 5% CO_2 to ensure that they were fully viable at the time of administration to rats. The time when >10% of cancer microcapsules burst was defined as the bursting day for each cell line. Two or 3 days before the bursting day was assumed to be the optimal time for portal injection. The histology of cancer microcapsules at the optimal day for portal injection was observed by embedding cancer microcapsules in optimum cutting temperature compound (Diagnostic Division, Miles, Inc., Elkhart, IN) and frozen sections were stained with H&E. To analyze the cell number included in each capsule at the optimal day for portal injection, microcapsules were sampled, enzymatically digested, and cells were counted using a hematocytometer.

Injection of Cancer Microcapsules in Nude Rats

Nude rats (male F344/NJcl-mu rats), 6 weeks of age with a weight of 100 to 125 g (Clea Japan, Tokyo, Japan), were employed. The rats were anesthetized by i.p. injection of pentobarbital, a midline incision was made, and the portal vein was exteriorized and linearized, thus enabling the insertion of a heparinized 20-gauge catheter (Terumo, Tokyo, Japan). A catheter was inserted at the very distal part of the mesenteric vein, near the cecum, and advanced 4 cm towards the liver and the tip of catheter was placed at the major trunk of the portal vein, with the point 5 to 8 mm near the liver hilum. The cancer microcapsules suspended in 1 mL saline were injected manually at ~0.1 mL/s and flushed with 0.5 mL of saline. The site where the catheter was inserted was ligated for hemostasis with 5-0 nylon sutures. Ligation of this point never caused intestinal necrosis because collateral vessel networks are well formed in the rat.

All animal experiments were done with the approval of the Animal Research Committee of the University of Tsukuba. Animals were maintained in a barrier facility on HEPA-filtered racks and fed with autoclaved laboratory rodent chow.

Liver Metastases Production by Portal Vein Injection of Cancer Microcapsules or Single Cell Suspension

To produce liver metastases in nude rats by injection of cancer microcapsules via the portal vein, 3,000 cancer microcapsules for each rat were administered: 12, 6, and 6 nude rats were employed for SUIT-2, AsPC-1, and BxPC-3 microcapsules, respectively. The same number of single cells included in 3,000 cancer microcapsules (2.1×10^6 for SUIT-2 and 4.5×10^6 for AsPC-1 and BxPC-3) were also injected via the portal vein. In order to inject a homogeneous single cell suspension, excluding cell aggregates or clumps, cell solutions were passed through a mesh strainer with a 40 μm pore size prior to administration. Six nude rats were employed for single cell injection of SUIT-2, AsPC-1, and BxPC-3, respectively. We assumed that the appropriate metastatic extent for evaluating the procedure would be ~10% to 20%. All rats were sacrificed at different times depending on the cell lines (SUIT-2 at 4 weeks, AsPC-1 at 6 weeks, and BxPC-3 at 5 weeks) with the intent of obtaining metastases with a suitable extent.

Evaluation of Sacrificed Nude Rats, Injected Cancer Microcapsules, or Single Cancer Cells

Incidence of liver metastases. To assess the potential for liver metastases, the incidence of liver metastases was evaluated macroscopically. The rate of liver metastases was defined as the number of rats positive for liver metastases divided by the number of experiments. Formalin-fixed, paraffin-embedded sections were subjected to microscopic examination.

Undesired metastases to sites other than the liver. To evaluate whether metastases occurred only in the liver, other organs and areas, i.e., peritoneal cavity, injection site, and lungs were carefully examined macroscopically. Any suspicious lesion was removed and subjected to histologic analysis.

Numerical evaluation of the extent of metastatic liver nodules: volumetric examination. In order to quantify the objective extent of liver metastases, a numeric calculation was employed. The metastatic extent was defined by the following formula: metastatic extent (%) = (metastatic volume / volume of entire liver) × 100. Formalin-fixed livers were divided into four lobes (left, middle, right, and caudate) and each lobe was then cut to a thickness of 2 mm. Next, the area of metastatic nodules in all serial sections was measured using image-processing software WinROOF (Mitani Corporation, Fukui, Japan). The metastatic volume and total volume of the liver were calculated by integration.

Variation of the Extent of Liver Metastases by Injecting Different Numbers of Cancer Microcapsules

To determine whether the extent of liver metastases varied according to the number of cancer microcapsules injected, various numbers of SUIT-2 microcapsules were injected. Five, 12, 7, and 8 nude rats were injected with 6,000, 3,000, 1,000, and 333 microcapsules, respectively, and both the incidence of liver metastases and the extent of tumor volume affected were calculated.

In vivo Sequential Observation of Cancer Microcapsule–Derived Liver Metastases

In order to assess the development of liver metastases from cancer microcapsules, livers were extracted from nude rats at days 3, 7, or 28 after portal injection of 3,000 SUIT-2 microcapsules. Livers were cut into serial 2 mm sections and stained with H&E to determine (*a*) distribution of cancer microcapsule, (*b*) status of microcapsules, i.e., whether capsules were ruptured or unruptured, and (*c*) distribution and size of liver metastases.

Pathophysiology of Liver Metastases: Cancer Microcapsules in Rats and Single Cell Injection in Mouse

The pathophysiology of liver metastases in nude rats generated by cancer microcapsules and those derived with conventional methods, i.e., injection

of single cells into the spleen in nude mouse were assessed. The following variables were evaluated: (*a*) macroscopic location of metastatic nodules, (*b*) microscopic histopathology of tumors, (*c*) desmoplastic reaction, and (*d*) neovascularization. Cancer microcapsule–derived liver metastases were assessed on day 28 in nude rats injected with 3,000 SUIT-2 microcapsules. Because single cell injection to the spleen of nude rats never generated liver metastases in our hands, nude mice were employed. Liver metastases derived from single cells were assessed 28 days after splenic injection of 2.1×10^6 cells/50 μL of SUIT-2 cells in nude mice. The macroscopic location and histopathology were analyzed using representative H&E stained slides. The extent of the desmoplastic reaction was compared by evaluation of collagen fibers visualized by Masson trichrome staining. Neovascularization was evaluated by the microvessel count (MVC) method as reported by Weidner et al., with minor modifications (24). Representative sections were stained immunohistochemically with anti–von Willebrand factor antibody (polyclonal rabbit anti-human factor VIII–related antigen; Dako Corporation, Santa Barbara, CA). The number of von Willebrand factor–positive vessels were counted and the average counts of five selected hotspots, i.e., the highest neovascularization areas in high power (×200) fields, were recorded as the MVC for each case (25).

Assessment of the Efficacy of Anticancer Drugs Using the Present Liver Metastases Rat Model

To investigate whether the rat liver metastases model was useful in evaluating the effect of anticancer drugs, 15 nude rats portally injected with 3,000 SUIT-2 microcapsules were randomly subdivided into three groups (five animals per group) on day 7. The first group was treated with gemcitabine (Gemzar, Eli Lilly, Indianapolis, IN) administrated via the dorsal vein at 80 mg/kg twice a week for 3 weeks (26). The second group was treated with irinotecan (Daiichi Pharmaceutical Co. Ltd., Tokyo, Japan) at a dose of 60 mg/kg twice a week for 3 weeks (10). The third control group received 0.5 mL saline solution twice a week for 3 weeks. All rats were sacrificed on day 28 and the extent of metastases was determined as described above.

Statistical Analyses

Differences in the metastatic rate between cancer microcapsules and single cell suspensions were analyzed using Fisher's exact test. Variations in the extent of liver metastases by injecting different numbers of cancer microcapsules were compared by one-way ANOVA. A $P < 0.05$ was considered statistically significant. Statistical calculations were done with the StatView software package (version 5.0, Abacus Concepts, Inc., Berkeley, CA).

Results

In vitro Culture of Cancer Microcapsules: Capsule Burst, Histology, and Cell Proliferation

The size of cancer microcapsules engineered in the present study was quite uniform (Fig. 1*A*). The average diameter of 100 randomly sampled microcapsules of SUIT-2, AsPC-1, and BxPC-3 microcapsules was 305 ± 39, 298 ± 21, and 362 ± 35 μm, respectively. Sequential *in vitro* observation of microcapsules showed that the cancer cells in microcapsules proliferated well and formed spheroids at days 5 to 7. Histologic observation of cancer

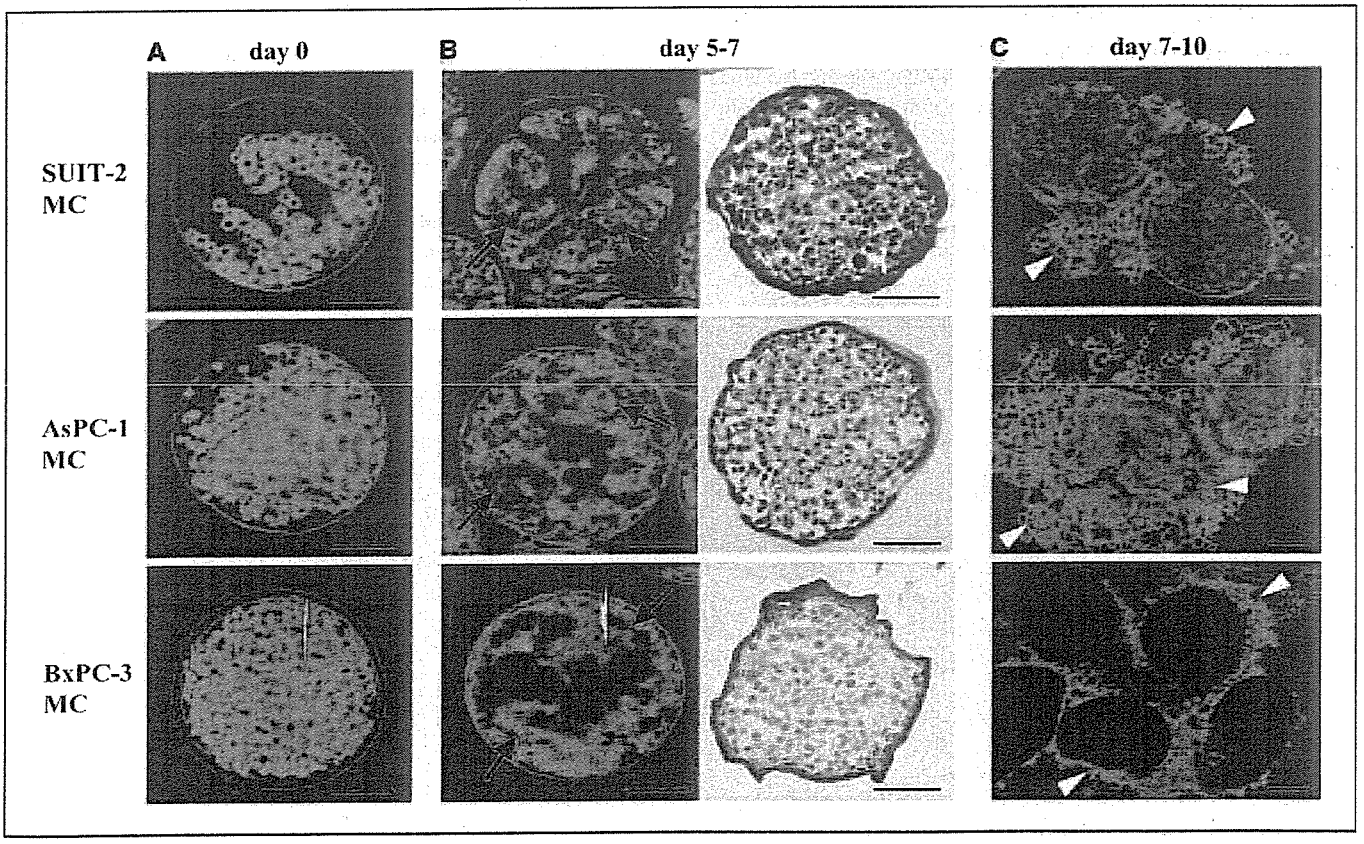

Figure 1. *In vitro* culture of cancer microcapsules: sequential observation and histology. Human pancreatic cells were encased in 300 μm alginate microcapsules using coaxial airflow (see Materials and Methods). *A*, representative pictures of cancer microcapsule from SUIT-2, AsPC-1, and BxPC-3 cells at day 0, immediately after production. *B*, after 5 to 7 days of *in vitro* incubation, cancer microcapsules were filled with proliferated cells forming spheroids (*arrows*). Histologic observation of frozen section stained with H&E of cancer microcapsules at the optimal day of portal injection showed three-dimensional proliferation of cancer cells. *C*, cancer microcapsules began to burst at days 7 to 10. Cancer cells, extruded from ruptured capsules continued to proliferate (*white arrowheads*). *Bars*, 100 μm.

microcapsules showed that all the cancer microcapsules proliferated in a three-dimensional manner (Fig. 1*B*). Further *in vitro* culture resulted in bursting of the outer layer of cancer microcapsules, and cancer cells were finally deviated outward and continued to grow in flasks (Fig. 1*C*). Although the speed of cell proliferation in cancer microcapsules differed between the three cell lines, all three cancer microcapsules burst nonetheless. The bursting times of SUIT-2, AsPC-1, and BxPC-3 microcapsules were on days 7, 7, and 10, respectively. From these results, the optimal day for portal injection of microcapsules from SUIT-2, AsPC-1, and BxPC-3 was assumed to be on days 5, 5, and 7, respectively. The average number of cells that were encased in one cancer microcapsule, at the optimal day for portal injection, was 718 cells for SUIT-2, 1,530 for AsPC-1, and 1,640 for BxPC-3.

Assessment of Liver Metastases Production in Nude Rats, Injected Cancer Microcapsules, or Single Cancer Cells

The metastatic potential to the liver of these three cell lines, by either single cell injection into the spleen and/or orthotopic implantation, has been reported to be different. SUIT-2 provides constant overt liver metastases (7). AsPC-1 is known to generate liver metastases, however, the extent of metastases is variable (7, 27). BxPC-3 does not cause liver metastases as reported by several authors (7, 17). Injection of three cancer microcapsules formed from different cell lines resulted in the successful production of overt liver metastases in all cases (Fig. 2).

Rate of liver metastases. The rate of liver metastases in rats injected with SUIT-2 microcapsules, AsPC-1 microcapsules, and BxPC-3 microcapsules was 100% (12 of 12), 100% (6 of 6), and 83% (5 of 6), respectively. In contrast, no liver metastases were formed by the injection of nonencapsulated single cancer cells (Table 1). Macroscopic observation and hepatic cross-sections showed that metastatic nodules tended to precipitate at peripheral hepatic margins (Fig. 2).

Metastases at organs other than the liver. No metastatic lesions other than in the liver were seen, and peritoneal, injection site, or pulmonary dissemination was not observed. However, occasional skin incisional wound metastases was seen in two rats that were injected with 3,000 SUIT-2 microcapsules (Table 1).

Numerical evaluation of the metastatic liver nodules: volumetric analyses. The metastatic extent to the liver produced by the injection of SUIT-2, AsPC-1, and BxPC-3 microcapsules was 14.6 (15.9/107.1 cm^3) ± 7.0%, 9.7 (11.4/113.2 cm^3) ± 5.8%, 15.0 (19.1/111.4 cm^3) ± 12.5%, respectively. The macroscopic extent of liver metastases is known to be larger than the calculated tumor volume. Our previous study showed that the tumor volume of clinically massive liver metastases remains ~10% to 30% when calculated by computed volumetry (28).

Control of the Extent of Liver Metastases by Injection of Varying Numbers of Cancer Microcapsules

The rate of liver metastases in rats injected with 6,000, 3,000, 1,000, and 333 microcapsules was 100% (5 of 5), 100% (12 of 12), 86% (6 of 7), and 50% (4 of 8), respectively. The extent of metastases in rats injected with 6,000, 1,000, and 333 microcapsules was 29.5 (46.0/146.2 cm^3) ± 13.1%, 1.9 (1.8/96.5 cm^3) ± 1.9%, 0.2 (0.2/88.4 cm^3) ± 0.3%, respectively (Fig. 3).

In vivo Sequential Observation of Liver Metastases Derived from Cancer Microcapsules

Distribution of cancer microcapsules at 3 days after portal injection in liver showed that two-thirds were lodged in the small peripheral (20–50 μm) portal veins, although one-third were trapped in the central wide (200–500 μm) portal vein (Fig. 4*a1*). It should be noted that 300 μm of microcapsules reached peripheral regions more than initially expected because the diameter of Glisson's sheath or the portal vein neighboring cancer microcapsules lodged were ~20 to 50 μm in diameter (Fig. 4*a2*). A total of 175 cancer microcapsules were observed in 10 representative slices on day 3, 35% (62 of 175) of which were ruptured. The proportion of ruptured microcapsules increased to 70% (88 of 128) at day 7 and 100% at day 28. Although intact cancer microcapsules should also be involved in the formation of metastatic foci, all cancer microcapsules at day 28 were assumed to be ruptured because almost all were buried in tumor nodules. Sequential

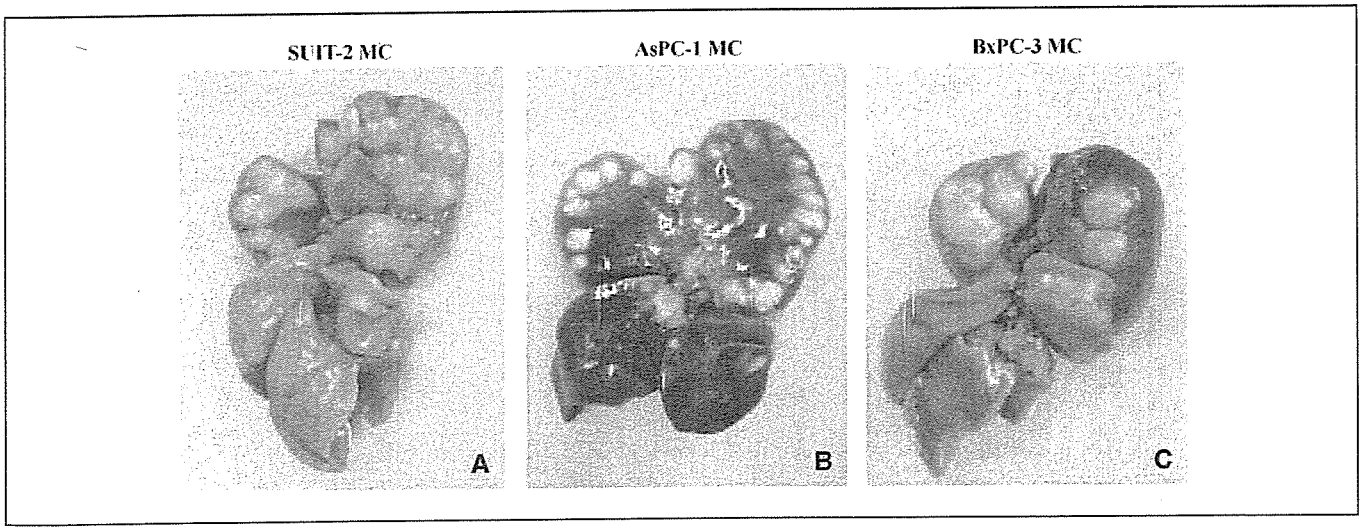

Figure 2. Overt liver metastases in nude rats by injection of three different human pancreatic cancer microcapsules via the portal vein. Representative gross appearance of rat livers at 28 days after injection of SUIT-2 microcapsules (*A*), 42 days after injection of AsPC-1 microcapsules (*B*), and 35 days after injection of BxPC-3 microcapsules (*C*). The hepatic metastatic extent produced by injection of SUIT-2, AsPC-1, and BxPC-3 microcapsules was 14.6 (15.9/107.1 cm^3) ± 7.0%, 9.7 (11.4/113.2 cm^3) ± 5.8%, and 15.0 (19.1/111.4 cm^3) ± 12.5%, respectively. Note that metastatic nodules, especially of AsPC-1 microcapsules, tended to precipitate at the peripheral regions of the liver.

Table 1. Liver metastasis take rate in rats by different injection form of cancer cells: cancer microcapsule versus single cells

	Cancer microcapsule*					Single cells†		
	n	Liver (rate %)	Peritoneum	Injection site	Lung	Wound	*n*	Liver	Others
SUIT-2	12	12 (100)	0	0	0	2	6	0	0
AsPC-1	6	6 (100)	0	0	0	0	6	0	0
BxPC-3	6	5 (83)	0	0	0	0	6	0	0

*Three thousand microcapsules with a 300 μm diameter were injected.
†A single cell suspension of 2.1 to 4.5 × 10^6 cancer cells were injected.

analysis of metastases revealed that cancer cells gradually extruded from the outer layer of the microcapsules at day 3, which could not be recognized macroscopically (Fig. 4*a2–3*). At day 7, metastatic foci developed to 0.5 to 2 mm, accounting for 6% of the sectional area (Fig. 4*b1*). Tumor growth was equally achieved with cancer microcapsules in both peripheral (Fig. 4*b2*) and central regions (Fig. 4*b3*). At day 28, overt liver metastases occupied 53% of the sectional area (Fig. 4*c1*) and were diffusely distributed from the peripheral to proximal regions (Fig. 4*c2–3*).

Pathophysiology of Liver Metastases: Cancer Microcapsules in Rats and Single Cell Injection in Mouse

Using both methods, metastatic foci were mainly distributed in the peripheral one-third of the hepatic hilum, i.e., marginal area of the liver (Fig. 5*a1* and *b1*). Microscopic observation of liver metastases from cancer microcapsules showed glandular formation around remnant microcapsules (Fig. 5*a2*). Single cell–derived liver metastases showed medullary proliferation of cancer cells

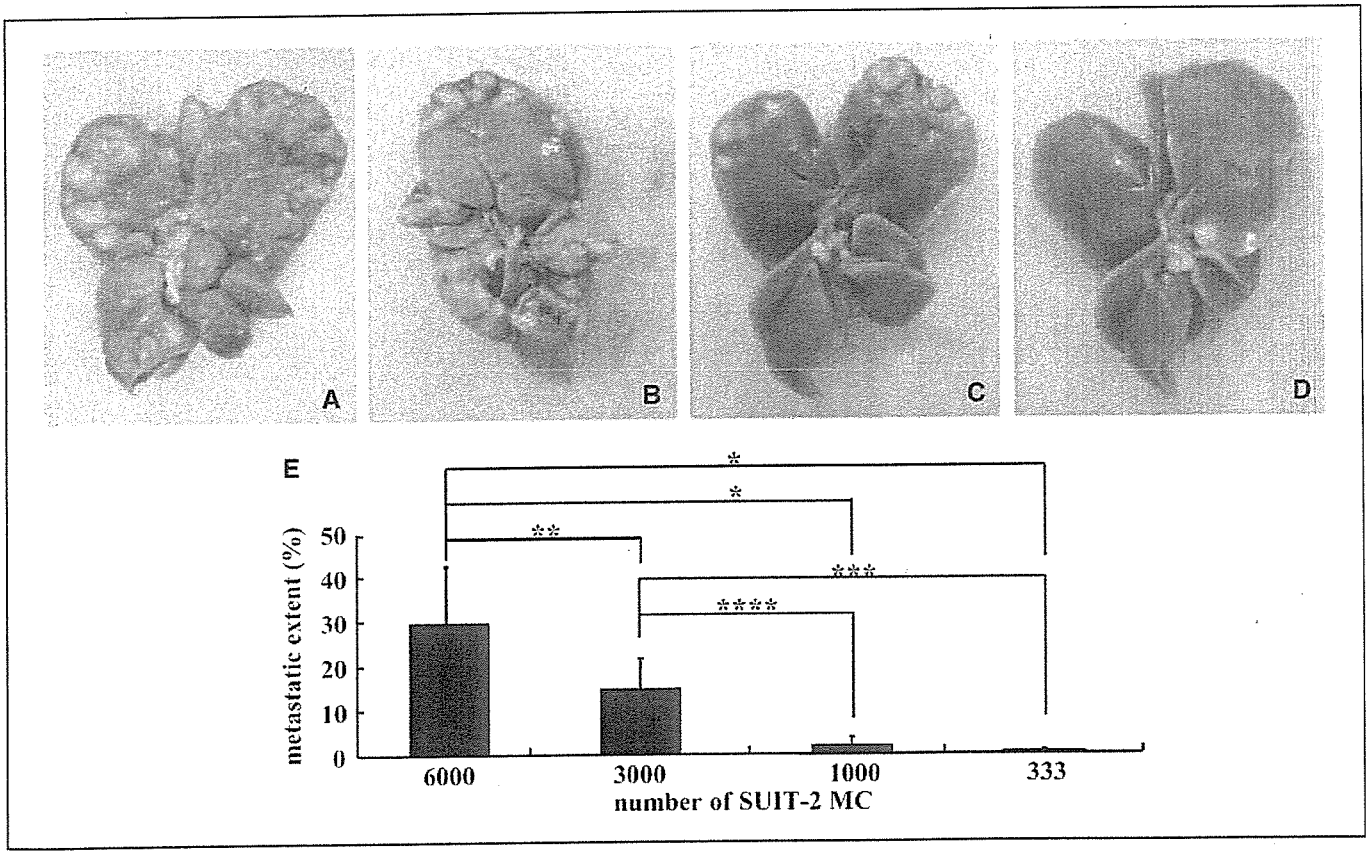

Figure 3. Intentional control of the extent of liver metastases by injecting different numbers of cancer microcapsules. Livers from nude rats 28 days after administration of 6,000 (*A*), 3,000 (*B*), 1,000 (*C*), and 333 (*D*) SUIT-2 microcapsules. *E*, the extent of liver metastases was numerically calculated (29.5% for 6,000 microcapsules, 14.6% for 3,000 microcapsules, 1.9% for 1,000 microcapsules, and 0.2% for 333 microcapsules), statistically demonstrating that the extent of liver metastases could be intentionally controlled by injecting different numbers of cancer microcapsules (*, $P < 0.0001$; **, $P = 0.0031$; ***, $P = 0.0009$; ****, $P = 0.049$).

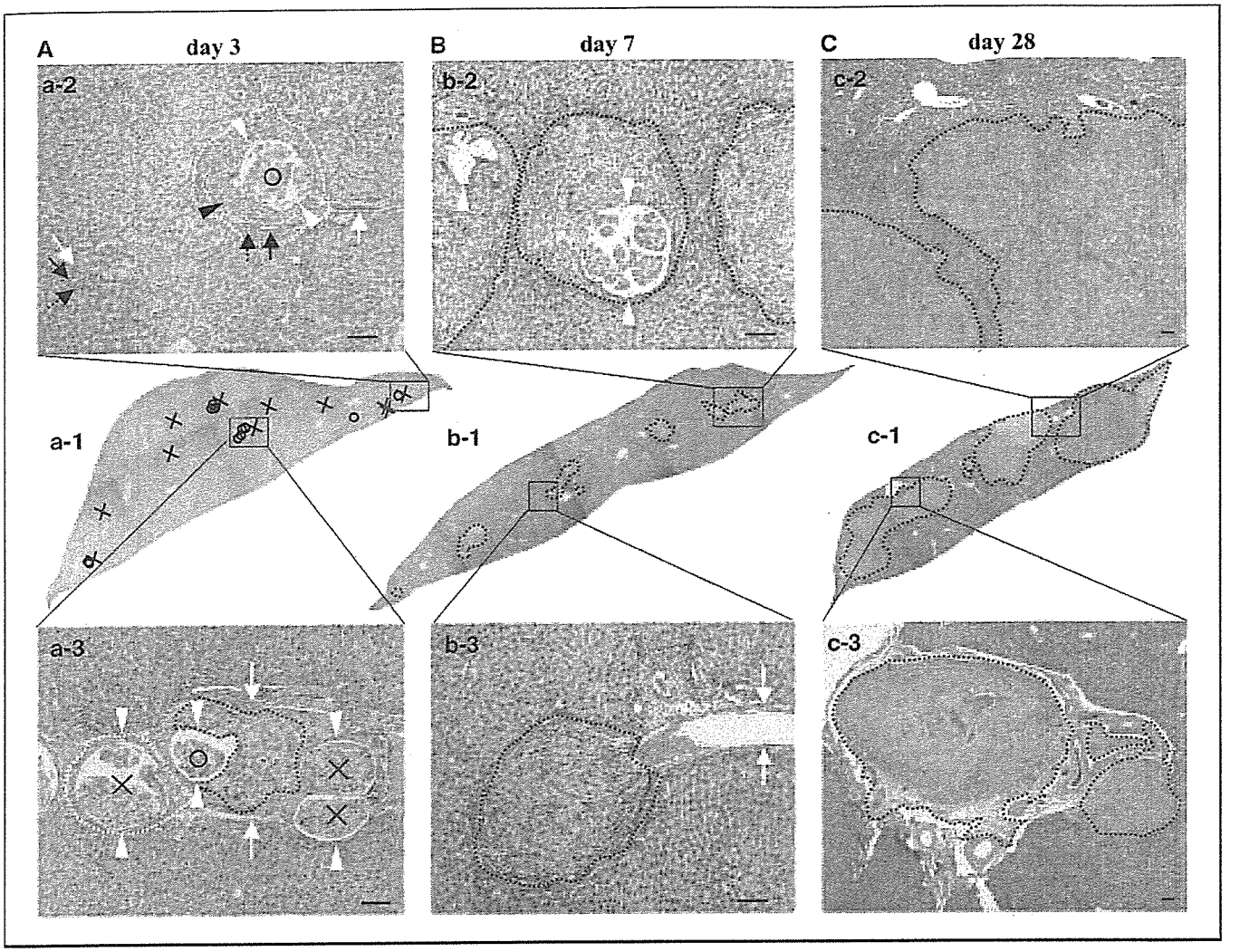

Figure 4. Sequential *in vivo* observation of liver metastases generated from cancer microcapsules. Representative pictures of rat liver, at day 3 (*A*), day 7 (*B*), and day 28 (*C*) after portal injection of 3,000 SUIT-2 microcapsules. *a1,* distribution of cancer microcapsules were marked on loupe observation (O, ruptured; ×, unruptured). Two-thirds of the microcapsules were lodged in peripheral small (20–50 μm) portal veins, although one-third were trapped in the central wide (200–400 μm) portal vein. *a2,* microscopic observation of the peripheral region on day 3, including a ruptured capsule. Outer layers of microcapsule (*white arrowheads*) and extruded cancer cell proliferation (*black arrowheads*). Fibroblastic proliferation around cancer microcapsules, a hallmark of the host reaction to foreign bodies, was sometimes observed at day 3 (*white dotted line*). It should be noted that 300 μm microcapsules reached regions much more peripheral than expected, because the diameter of the portal vein in Glisson's sheath (*white arrow*) neighboring lodged cancer microcapsules were ~20 to 50 μm in diameter. Peripheral bile ducts (*black arrow*), hepatic arteries (*black dotted arrows*). *a3,* microscopic observation of the central region at day 3. Four microcapsules, one marked with an "O" was ruptured and three marked with an "×" were unruptured and trapped in the large portal vein (400 μm), on both sides (*white arrows*). Extruded cancer cells beginning to proliferate (*black dotted line*). *b1,* loupe observation at day 7. Recognizable metastatic foci of 0.5 to 2.0 mm accounting for a sectional area of 6% (*surrounded by a dotted line*). *b2,* microscopic observation of peripheral regions showed noteworthy proliferation of cancer cells (*black dotted line*) around microcapsules (*white arrowheads*). *b3,* microscopic observation of the central region showed metastatic foci at the tip of a 120 μm portal vein (*two white arrows*). *c1,* loupe observation at day 28. Liver metastatic foci, which occupy a sectional area of 53%, were diffusely observed from the proximal to the peripheral area of the liver. *c2,* microscopic observation of the peripheral region and (*c3*) the central region showed that cancer microcapsules and fibrotic proliferation were surpassed by cancer cells and could not be recognized in mature metastatic foci.

with a cellularity of >90% and no glandular formation (Fig. 5*b2*). The desmoplastic reaction, proliferation of interstitial collagens, visualized by Masson trichrome staining was more evident in liver metastases originating from cancer microcapsules (Fig. 5*a3* and *b3*). The desmoplastic reaction was heterogeneously distributed in the liver metastases from cancer microcapsules. Dense collagen proliferations predominantly distributed the surrounding areas of cancer microcapsule remnants, presumably due to a foreign body reaction to the extracellular components of the microcapsules. Regarding neovascularity, the MVC of cancer microcapsules and single cell–derived metastases were 30.4 ± 7.0, and 62.8 ± 14.4, respectively.

Application of Liver Metastases Model for Evaluation of Anticancer Drug Efficacy

The extent of metastases in rats treated with gemcitabine, irinotecan, or saline was 0.52 (0.44/82.2 cm^3) ± 0.72%, 0.12 (0.1/80.6 cm^3) ± 0.16%, and 23.7 (26.6/106.4 cm^3) ± 11.3%, respectively. Objective evaluation for anticancer drug efficacy was possible because undesired metastases to organs other than liver was not observed.

Discussion

The present cancer microcapsule method led to the successful and efficient production of liver metastasis in rats. The mechanism

for successful production of liver metastases may be explained by the following considerations. First, cancer cells are forcibly trapped (mechanically embolized) because the microcapsules were large enough not to pass through the liver. Secondly, the cancer cells delivered to the implantation sites were fully viable. Lastly, embolization of cancer microcapsules to the peripheral portal vein mediates local ischemia, releasing cytokines and/or growth factors.

Cancer cell implantation in the liver is believed to occur at the sinusoids, and the principal mechanism is binding between cell surface adhesion molecules of single cancer cells and receptor molecules on hepatic endothelial cells (29). We assumed that an additional factor likely to be equally important is the mechanical entrapment of cancer cell clumps at the peripheral portal vein. The diameter of the portal vein of nude rats at the liver hilum is ~1 mm and gradually narrows to 20 to 50 μm before going to the periphery of the liver. Sequentially, the peripheral portal vein shifts to the liver sinusoids, i.e., the space between hepatocytes, the diameter of which is 7 μm. The size of a single cancer cell is ~8.3 to 47 μm (30), and a previous study has shown that large cancer cells are advantageous in liver implantation (31). Once cancer cells form aggregates, the size might increase to ~30 to 50 μm (32). Larger aggregates, compared with cell suspensions, are known to be more effective in both implantation and survival to form gross tumor colonies after i.v. injection (33, 34). In order to improve the ratio of cell aggregates, previous experimental models

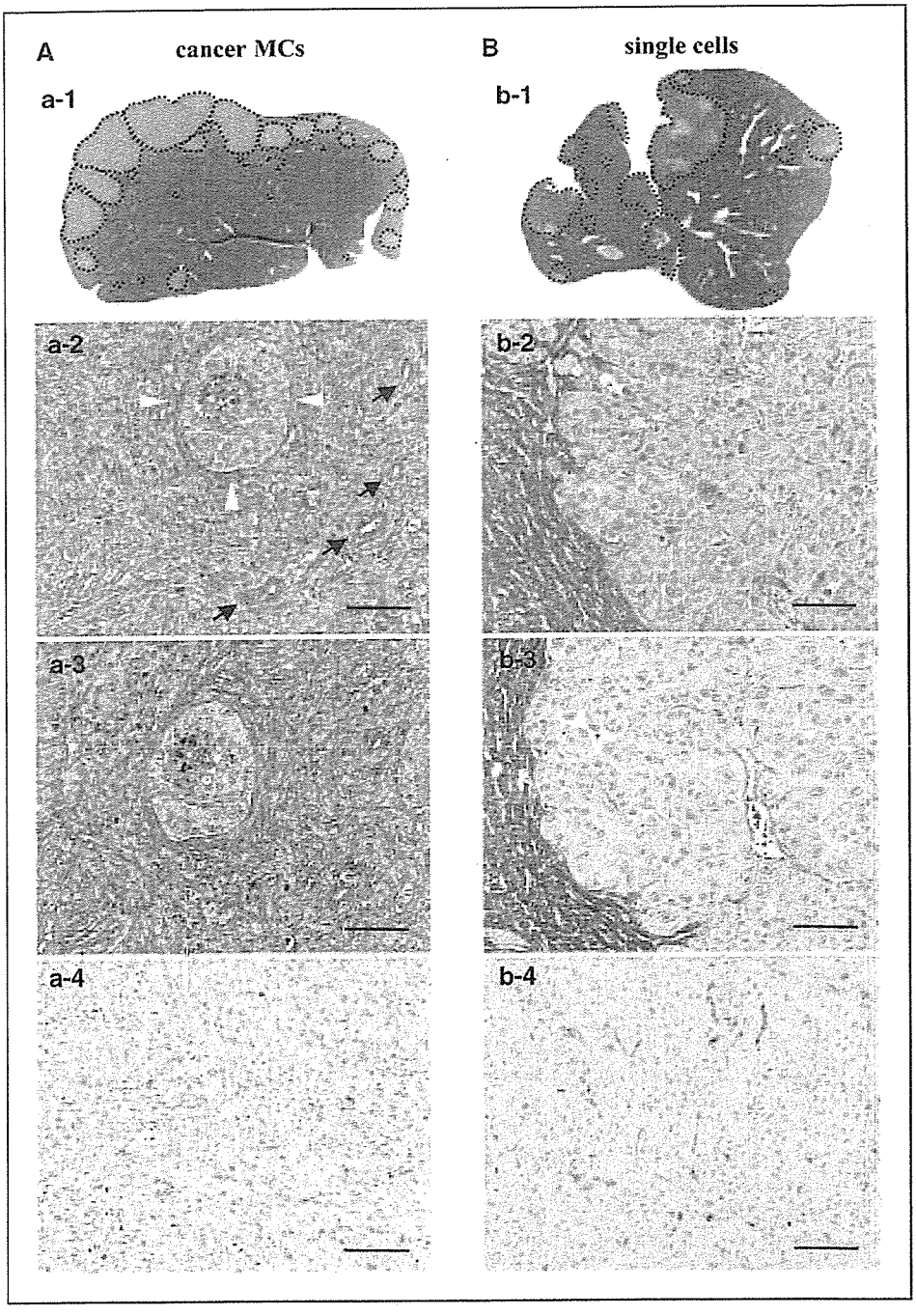

Figure 5. Pathophysiologic assessment of liver metastases generated by cancer microcapsules in rats versus single cell injection in mice. Histopathologic and immunohistochemical findings of SUIT-2 liver metastases, 28 days after administration of 3,000 cancer microcapsules in a nude rat (*A*) and single cell suspension (2.1×10^6 cells) in a nude mouse (*B*). *a1* and *b1*, macroscopic image stained with H&E shows that metastatic nodules (*surrounded by a dotted line*) tend to form at the peripheral margin of the liver in both methods. *a2*, microscopic observation of cancer microcapsule–derived liver metastases showed glandular formation (*arrows*) around remnant microcapsule (*white arrowheads*), indicating a histologic presentation similar to that of primary pancreatic cancer. *b2*, microscopic observation of liver metastases derived from single cells showed that medullary proliferation of cancer cells with a cellularity of >90% with no glandular formation that is not histologically similar to primary pancreatic cancer. *a3* and *b3*, proliferation of interstitial collagens, visualized by Masson trichrome staining, was more evident in liver metastases derived from cancer microcapsules than in those from single cell suspensions. *a4* and *b4*, the extent of neovascularity was evaluated by the MVC method using anti–factor VIII antibodies. The MVC of cancer microcapsule and single cell–derived metastases was 30.4 ± 7.0, and 62.8 ± 14.4, respectively. Liver metastases with cancer microcapsules were less vascularized with respect to those derived using a single cell suspension. *Bars*, 100 μm.

have employed an *in vitro* rotary cell culture system (35–37). In these models, however, the size and number of cancer cells included in these aggregates varies greatly. Furthermore, these cell aggregates are physically fragile and are easily damaged by transplantation before arriving to potential implantation sites. As a result, the frequency of liver metastases by this method ranges from 20% to 40% even under optimal conditions (36, 38). Moreover, only a highly limited number of cell lines are capable of forming aggregates in this *in vitro* system, greatly limiting their utility. We used uniform cancer microcapsules with a diameter of 300 μm, which resulted in 100% of the injected cancer microcapsules becoming trapped in the peripheral portal vein, and thus, never pass through the liver sinusoids to the hepatic vein.

A second advantage of cancer microcapsules may be their capacity to deliver viable cancer cells to implantation sites. When suspensions of cancer cells are injected via the portal vein or spleen in animals, the cells are rapidly attacked by the host immune system and also suffer from hemodynamic forces (39). In fact, although the majority of injected cancer cells were found to be arrested in the liver sinusoid several minutes after injection, the vast majority of injected cancer cells were disseminated or no longer viable at 24 hours. Finally, only 1% of injected cancer cells survive in the liver, and further progression to form metastatic foci is even less probable (40, 41). Although observation by intravital video microscopy showed that melanoma cells can survive in the liver (>36% even at day 13; ref. 42), it seems reasonable to assume that, in general, relatively few cells are the seeds of metastases. In our cancer microcapsules, cells were preincubated *ex vivo* until the logarithmic growth phase and were effectively protected by the outer layer of the microcapsule throughout the processes of initial administration, delivery, embolization, and growth before bursting. Physical protection by the microcapsule may beneficial, although this may not be necessary in all cell types, increasing the ratio of viable cells in liver and therefore aiding in the formation of metastases.

The third mechanism that may explain the success of the present liver metastatic model may be related to liver ischemia, which induces the release of cytokines and/or growth factors, simultaneously possess the potential to stimulate cancer cell growth (43–45). It is quite reasonable to assume that once cancer microcapsules are embolized, more peripheral liver parenchyma will be included in ischemic environments. There is also clinical evidence that hepatic pedicle clamping during liver surgery causes liver ischemia and mediates the release of cytokines such as tumor necrosis factor α, interleukin 1β, and other growth factors, accelerating cancer growth (46–48). Together with these results, we assume that local ischemia of transplanted sites of the liver might contribute, at least in part, to the successful production of overt metastases.

One question that arises is whether the pathophysiology of liver metastases generated by the present cancer microcapsule method is equivalent to that of widely used liver metastases generated by single cell injection. It should be highlighted that liver metastasis using the cancer microcapsule method has only been tested in rats and successful liver metastasis by single cell injection using certain special cells (SUIT-2, in the present report) was observed only in mice; therefore, histopathologic comparisons were made using different species. Regarding the region of liver metastases production, this method is initially expected to provide artificially proximal tumors, located in the proximity of the wide portal vein which has a diameter of 300 μm. In reality, however, the regions of cancer microcapsules embolized were distributed more peripherally than expected, resulting in the precipitation of metastatic nodules in the marginal area of the liver. The fact that 300 μm of cancer microcapsules were found at the 20 to 50 μm peripheral portal vein shows the considerable plasticity of the portal vein. There were some cancer microcapsules that were likely to have been trapped in the central area, where the diameter of the portal veins ranges from 200 to 400 μm. Metastatic formation in the central region, however, was not a phenomenon specific to the cancer microcapsule method because they were also observed following single cell injection. Regarding the region of liver metastases, therefore, cancer microcapsules confer a similar hepatic distribution in rats to that of conventional single cell injection in mice.

Almost invariably, the histopathology of tumors in animal models is quite different from that of primary, clinical cancer specimens. Pancreatic cancer is well-known for its hypovascular nature and extensive desmoplastic reaction. Tumors in single cell–derived liver metastases in mice usually show endocrine tumor–like growth with an expansive growth pattern, without the formation of glands. Given this, it was unexpected that tumors generated by cancer microcapsules in rats formed glands around fibroblasts. Because cancer cells are known to be heavily affected by surrounding fibroblasts and infiltrating hematopoietic cells (49), the presence of a foreign body reaction to cancer microcapsules also seemed to be beneficial in mimicking the histopathology of primary pancreatic cancer. Together with the unique characteristics of the present animal model, such as stable production of liver metastases and the presence of metastases only in liver, this presents immense advantages in evaluating the effect of therapeutics aimed at controlling liver metastases. In fact, the effectiveness of commonly used anticancer chemotherapeutic agents can be evaluated in an objective and quantitative manner.

Although we succeeded in producing consistent liver metastases in rats using cell lines with little or no metastatic potential (AsPC-1, BxPC-3), it is unknown if the cancer microcapsule method will be applicable to all cell lines and will always produce overt liver metastases. The necessary conditions for liver metastases in the present microcapsule system are that cancer cells have two capabilities. The first is a growth potential that is powerful enough to burst the outer layer of the microcapsule, whereas the second is the ability to proliferate in liver parenchyma after being extruded from the ruptured microcapsule. The first condition may be enhanced by the unique application of the present method, i.e., the ability of coencapsulation with different cells or substances. Matrigel, an extracellular matrix that contains several growth factors and cytokines, was used as a "burst-supporting" agent in the present study, although coculture with various growth factors, cytokines, extracellular matrix components, and fibroblasts might also augment cell proliferation and capsule burst. Regarding the second condition, some cancer cells have never been reported to proliferate in liver even after direct intrahepatic injection, indicating that the liver is not an appropriate soil for some cell lines (18, 50). Application of the present microcapsule system to those cell lines might not generate liver metastases, even if they have the capacity to rupture the outer layer of microcapsules.

In conclusion, we succeeded in producing consistent overt liver metastases in nude rats using cancer microcapsules with a diameter of 300 μm, whereas the administration of single cancer cells never produced liver metastases in rats. Although the

advantage of this microcapsule method has been shown here in rats, this method may be applicable for larger animals such as rabbits, dogs, and pigs. In smaller animals such as mice, liver metastasis production was possible with the single cell injection method only if we used certain cancer cell lines. The present cancer microcapsule method may be useful for obtaining liver metastases in mice, especially for cell lines that will not form liver metastases with conventional methods. It should be noted, however, that technical improvements such as the production of smaller (<100 μm) cancer microcapsules and better surgical skill in injecting cancer microcapsules to the narrow portal vein, and especially the hemostasis step after injection, are necessary for applying the present method in mice. Even though the present microcapsule system is artificial, this may nonetheless provide information for understanding the mechanism of clinical liver metastases, highlighting the importance of anatomical-mechanical entrapment. We believe that the present cancer microcapsule method could contribute to the development of new anticancer therapeutics by providing consistent tumor growth in animal models.

Acknowledgments

Received 1/31/2006; revised 9/12/2006; accepted 9/22/2006.

Grant support: Supported in part by a Grant-in-Aid for Cancer Research (15 S-1) from the Ministry of Health, Labour, and Welfare, and in part by a Grant-in-Aid for Scientific Research (KAKENHI, 17659400) from The Ministry of Education, Culture, Sports, Science, and Technology of Japan.

The costs of publication of this article were defrayed in part by the payment of page charges. This article must therefore be hereby marked *advertisement* in accordance with 18 U.S.C. Section 1734 solely to indicate this fact.

We thank Dr. Patrick Moore for help in editing the manuscript.

References

1. Mao C, Domenico DR, Kim K, Hanson DJ, Howard JM. Observations on the developmental patterns and the consequences of pancreatic exocrine adenocarcinoma. Findings of 154 autopsies. Arch Surg 1995;130:125–34.
2. Stangl R, Altendorf-Hofmann A, Charnley RM, Scheele J. Factors influencing the natural history of colorectal liver metastases. Lancet 1994;343:1405–10.
3. Kozlowski JM, Fidler IJ, Campbell D, et al. Metastatic behavior of human tumor cell lines grown in the nude mouse. Cancer Res 1984;44:3522–9.
4. Vezeridis MP, Meitner PA, Tibbetts LM, et al. Heterogeneity of potential for hematogenous metastasis in a human pancreatic carcinoma. J Surg Res 1990;48:51–5.
5. Morikawa K, Walker SM, Jessup JM, Fidler IJ. *In vivo* selection of highly metastatic cells from surgical specimens of different primary human colon carcinomas implanted into nude mice. Cancer Res 1988;48:1943–8.
6. Yasoshima T, Denno R, Kawaguchi S, et al. Establishment and characterization of human gastric carcinoma lines with high metastatic potential in the liver: changes in integrin expression associated with the ability to metastasize in the liver of nude mice. Jpn J Cancer Res 1996;87:153–60.
7. Takamori H, Hiraoka T, Yamamoto T. Expression of tumor-associated carbohydrate antigens correlates with hepatic metastasis of pancreatic cancer: clinical and experimental studies. Hepatogastroenterology 1996;43:748–55.
8. Ohta T, Futagami F, Arakawa H, et al. [Inhibitory effect of FOY-305 on liver metastasis of the pancreatic cancer]. Gan To Kagaku Ryoho 1996;23:1669–72.
9. Tibbetts LM, Doremus CM, Tzanakakis GN, Vezeridis MP. Liver metastases with 10 human colon carcinoma cell lines in nude mice and association with carcinoembryonic antigen production. Cancer 1993;71:315–21.
10. Takiguchi S, Kumazawa E, Shimazoe T, Tohgo A, Kono A. Antitumor effect of DX-8951, a novel camptothecin analog, on human pancreatic tumor cells and their CPT-11-resistant variants cultured in vitro and xenografted into nude mice. Jpn J Cancer Res 1997;88:760–9.
11. O'Reilly MS, Holmgren L, Chen C, Folkman J. Angiostatin induces and sustains dormancy of human primary tumors in mice. Nat Med 1996;2:689–92.
12. Kisker O, Onizuka S, Banyard J, et al. Generation of multiple angiogenesis inhibitors by human pancreatic cancer. Cancer Res 2001;61:7298–304.
13. Tan MH, Holyoke ED, Goldrosen MH. Murine colon adenocarcinoma: syngeneic orthotopic transplantation and subsequent hepatic metastases. J Natl Cancer Inst 1977;59:1537–44.
14. Marincola F, Taylor-Edwards C, Drucker B, Holder WD, Jr. Orthotopic and heterotopic xenotransplantation of human pancreatic cancer in nude mice. Curr Surg 1987;44:294–7.
15. Fu X, Guadagni F, Hoffman RM. A metastatic nude-mouse model of human pancreatic cancer constructed orthotopically with histologically intact patient specimens. Proc Natl Acad Sci U S A 1992;89:5645–9.
16. Furukawa T, Kubota T, Watanabe M, Kitajima M, Hoffman RM. A novel "patient-like" treatment model of human pancreatic cancer constructed using orthotopic transplantation of histologically intact human tumor tissue in nude mice. Cancer Res 1993;53:3070–2.
17. Aubert M, Panicot L, Crotte C, et al. Restoration of α(1,2) fucosyltransferase activity decreases adhesive and metastatic properties of human pancreatic cancer cells. Cancer Res 2000;60:1449–56.
18. Kuo TH, Kubota T, Watanabe M, et al. Liver colonization competence governs colon cancer metastasis. Proc Natl Acad Sci U S A 1995;92:12085–9.
19. Pajet S. The distribution of secondary growths in cancer of the breast. Lancet 1889;1:571–3.
20. Ewing J. Neoplastic disease. A treatise on tumors. 3rd ed. Philadelphia: Saunders; 1928.
21. Lim F, Sun AM. Microencapsulated islets as bioartificial endocrine pancreas. Science 1980;210:908–10.
22. Iwamura T, Katsuki T, Ide K. Establishment and characterization of a human pancreatic cancer cell line (SUIT-2) producing carcinoembryonic antigen and carbohydrate antigen 19-9. Jpn J Cancer Res 1987;78:54–62.
23. Van Raamsdonk JM, Chang PL. Osmotic pressure test: a simple, quantitative method to assess the mechanical stability of alginate microcapsules. J Biomed Mater Res 2001;54:264–71.
24. Weidner N, Semple JP, Welch WR, Folkman J. Tumor angiogenesis and metastasis-correlation in invasive breast carcinoma. N Engl J Med 1991;324:1–8.
25. Ueda T, Oda T, Kinoshita T, et al. Neovascularization in pancreatic ductal adenocarcinoma: microvessel count analysis, comparison with non-cancerous regions and other types of carcinomas. Oncol Rep 2002;9:239–45.
26. Schultz RM, Merriman RL, Toth JE, et al. Evaluation of new anticancer agents against the MIA PaCa-2 and PANC-1 human pancreatic carcinoma xenografts. Oncol Res 1993;5:223–8.
27. Kusama T, Mukai M, Iwasaki T, et al. 3-Hydroxy-3-methylglutaryl-coenzyme A reductase inhibitors reduce human pancreatic cancer cell invasion and metastasis. Gastroenterology 2002;122:308–17.
28. Nakahashi C, Oda T, Kinoshita T, et al. The impact of liver metastasis on mortality in patients initially diagnosed with locally advanced or resectable pancreatic cancer. Int J Gastrointest Cancer 2003;33:155–64.
29. Honn KV, Tang DG. Adhesion molecules and tumor cell interaction with endothelium and subendothelial matrix. Cancer Metastasis Rev 1992;11:353–75.
30. Thorlacius H, Prieto J, Raud J, et al. Tumor cell arrest in the microcirculation: lack of evidence for a leukocyte-like rolling adhesive interaction with vascular endothelium *in vivo*. Clin Immunol Immunopathol 1997;83:68–76.
31. Mizuno N, Kato Y, Shirota K, et al. Mechanism of initial distribution of blood-borne colon carcinoma cells in the liver. J Hepatol 1998;28:878–85.
32. Roberts S, Watne A, McGrath R, McGrew E, Cole WH. Technique and results of isolation of cancer cells from the circulating blood. AMA Arch Surg 1958;76:334–46.
33. Fidler IJ. Tumor heterogeneity and the biology of cancer invasion and metastasis. Cancer Res 1978;38:2651–60.
34. Liotta LA, Saidel MG, Kleinerman J. The significance of hematogenous tumor cell clumps in the metastatic process. Cancer Res 1976;36:889–94.
35. Topal B, Roskams T, Fevery J, Penninckx F. Aggregated colon cancer cells have a higher metastatic efficiency in the liver compared with nonaggregated cells: an experimental study. J Surg Res 2003;112:31–7.
36. van der Elst J, De Greve J, Geerts F, et al. Quantitative study of liver metastases from colon cancer in rats after treatment with cyclosporine A. J Natl Cancer Inst 1986;77:227–32.
37. Panis Y, Ribeiro J, Chretien Y, Nordlinger B. Dormant liver metastases: an experimental study. Br J Surg 1992;79:221–3.
38. Panis Y, Nordlinger B, Delelo R, et al. Experimental colorectal liver metastases. Influence of sex, immunological status and liver regeneration. J Hepatol 1990;11:53–7.
39. Weiss L. The hemodynamic destruction of circulating cancer cells. Biorheology 1987;24:105–15.
40. Fidler IJ. Metastasis: quantitative analysis of distribution and fate of tumor emboli labeled with 125 I-5-iodo-2′-deoxyuridine. J Natl Cancer Inst 1970;45:773–82.
41. Barbera-Guillem E, Smith I, Weiss L. Cancer-cell traffic in the liver. II. Arrest, transit and death of B16F10 and M5076 cells in the sinusoids. Int J Cancer 1993;53:298–301.
42. Luzzi KJ, MacDonald IC, Schmidt EE, et al. Multistep nature of metastatic inefficiency: dormancy of solitary cells after successful extravasation and limited survival of early micrometastases. Am J Pathol 1998;153:865–73.
43. Kimura N, Muraoka R, Horiuchi T, et al. Intermittent hepatic pedicle clamping reduces liver and lung injury. J Surg Res 1998;78:11–7.
44. Yoshida M, Horiuchi T, Uchinami M, et al. Intermittent hepatic ischemia-reperfusion minimizes liver metastasis in rats. J Surg Res 2003;111:255–60.
45. Ramadori G, Armbrust T. Cytokines in the liver. Eur J Gastroenterol Hepatol 2001;13:777–84.
46. Doi K, Horiuchi T, Uchinami M, et al. Hepatic ischemia-reperfusion promotes liver metastasis of colon cancer. J Surg Res 2002;105:243–7.
47. van der Bilt JD, Kranenburg O, Nijkamp MW, et al. Ischemia/reperfusion accelerates the outgrowth of hepatic micrometastases in a highly standardized murine model. Hepatology 2005;42:165–75.
48. Ku Y, Kusunoki N, Shiotani M, et al. Stimulation of haematogenous liver metastases by ischaemia-reperfusion in rats. Eur J Surg 1999;165:801–7.
49. Bingle L, Brown NJ, Lewis CE. The role of tumour-associated macrophages in tumour progression: implications for new anticancer therapies. J Pathol 2002;196:254–65.
50. Yasui N, Sakamoto M, Ochiai A, et al. Tumor growth and metastasis of human colorectal cancer cell lines in SCID mice resemble clinical metastatic behaviors. Invasion Metastasis 1997;17:259–69.

Radiotherapy and Oncology 80 (2006) 93–97
www.thegreenjournal.com

Treatment of lung damage

Retrospective analysis of steroid therapy for radiation-induced lung injury in lung cancer patients

Ikuo Sekine[a,*], Minako Sumi[b], Yoshinori Ito[b], Hiroshi Nokihara[a], Noboru Yamamoto[a], Hideo Kunitoh[a], Yuichiro Ohe[a], Tetsuro Kodama[a], Nagahiro Saijo[a], Tomohide Tamura[a]

[a]*Division of Internal Medicine and Thoracic Oncology, and* [b]*Division of Radiation Oncology, National Cancer Center Hospital, Tokyo, Japan*

Abstract

Purpose: To disclose characteristics of lung cancer patients developing radiation-induced lung injury treated with or without corticosteroid therapy.

Methods and materials: Radiographic changes, symptoms, history of corticosteroid prescription, and clinical course after 50–70 Gy of thoracic radiotherapy were retrospectively evaluated in 385 lung cancer patients.

Results: Radiation-induced lung injury was stable without corticosteroid in 307 patients (Group 1), stable with corticosteroid in 64 patients (Group 2), and progressive to death despite corticosteroid in 14 patients (Group 3). Fever and dyspnea were noted in 11%, 50% and 86% ($p < 0.001$), and in 13%, 44% and 57% ($p < 0.001$) patients in Groups 1–3, respectively. Median weeks between the end of radiotherapy and the first radiographic change were 9.9, 6.7 and 2.4 for Groups 1–3, respectively ($p < 0.001$). The initial prednisolone equivalent dose was 30–40 mg daily in 52 (67%) patients. A total of 16 (4.2%) patients died of radiation pneumonitis or steroid complication with a median survival of 45 (range, 8–107) days.

Conclusion: Development of fever and dyspnea, and short interval between the end of radiotherapy and the first radiographic change were associated with fatal radiation-induced lung injury. Prednisolone 30–40 mg daily was selected for the treatment in many patients.

 Radiotherapy and Oncology 80 (2006) 93–97.

Keywords: Radiation pneumonitis; Radiotherapy; Lung cancer; Corticosteroid

Thoracic radiotherapy is widely used for the curative and palliative treatment of lung cancer. Radiation-induced lung injury was first described as early as 1922 [1,2], and two types of lung injury, radiation pneumonitis and radiation fibrosis, were recognized in 1925 [3]. Radiation pneumonitis occurs in 5–15% of patients who have received radiation therapy for lung cancer. Its clinical symptoms are characterized by cough, dyspnea and fever developing between 1 and 3 months after the end of radiotherapy. Distinctive radiographic changes of radiation pneumonitis are a ground-glass opacification or diffuse haziness in early phase, and then alveolar infiltrates or dense consolidation in late phase in the region corresponding to the irradiated area [4–7]. Radiation pneumonitis may persist for a month or more and subside gradually. In severe cases, however, pneumonitis progresses to death due to respiratory failure within few weeks [4].

Use of adrenocorticotropic hormone (ACTH) and cortisone for radiation pneumonitis in a case was first reported in 1951 [8], and 9 cases of radiation pneumonitis treated with cortisone therapy in the literature were reviewed in 1968 [9]. Although no case series or clinical trials of corticosteroid therapy have been reported since that time, prednisolone has been given in patients with severe pneumonitis in clinical practice. The initial dose of prednisolone, approximately 30–100 mg daily, and very slow tapering schedule are in agreement among experts [4–6,10], because early withdrawal results in aggravation of pneumonitis [11–13]. There is no consensus, however, about criteria to define when steroids are required for radiation-induced lung injury. The objective of this study is to disclose general characteristics of lung cancer patients developing radiation-induced lung injury treated with or without corticosteroid therapy, to obtain data on the initiation criteria, dose, and taper schedule of corticosteroid therapy for further prospective trials.

Patients and methods

Consecutive lung cancer patients treated with thoracic radiotherapy at a total dose of 50–70 Gy in National Cancer

0167-8140/$ - see front matter doi:10.1016/j.radonc.2006.06.007

Center Hospital between January 1998 and December 2003 were subjects of this study. We retrospectively reviewed all chest X-ray films taken during 6 month period from the end of thoracic radiation to identify the first radiographic change and its progress. History of corticosteroid prescription, symptoms at the time of and one-month period after the first radiographic change in a chest X-ray film, and clinical course of radiation-induced lung injury were obtained from medical charts. The diagnosis of radiation-induced lung injury was defined as radiographic changes including opacification, diffuse haziness, infiltrates or consolidation conforming to the outline of the sharply demarcated irradiated area in a chest X-ray film. During clinical course, scarring (fibrosis) was developed within the irradiated area leading to a reduction in lung volume. In contrast, pulmonary infection spreads through anatomical structure of the lung, and the boundary of infiltrates corresponds to anatomical boundary of the lung. For patients with fever, the radiographical response to antibiotics was also evaluated. Observed differences in the proportions of patients in various patient subgroups were evaluated using Chi-square test. Differences between continuous variables were compared using Mann–Whitney tests. The Dr. SPSS II 11.0 for Windows software package (SPSS Japan Inc., Tokyo, Japan) was used for all statistical analyses.

Results

Of 544 lung cancer patients receiving thoracic radiotherapy at a total dose of 50–70 Gy, 111 patients were excluded from this study because they were not evaluable: loss of follow-up in 88 patients, early lung cancer progression in 18 patients, chemotherapy-induced neutropenic fever and pneumonia in three patients, death of bleeding from the esophageal stent in one patient, and no chest X-ray films available in one patient. In addition, 48 patients (11% of 433 evaluable patients) were also excluded because no radiation-induced lung injury was noted. Thus, the subject of this study was 385 patients.

Of the 385 patients, 78 (20%) received corticosteroid therapy for radiation-induced lung injury, and 307 did not. Radiation-induced lung injury was stable without corticosteroid in the 307 (80%) patients (Group 1), stable or in remission with corticosteroid in 64 (17%) patients (Group 2), and progressive to death despite corticosteroid in 14 (4%) patients (Group 3). No difference in sex, total dose, intent of radiotherapy, and combination chemotherapy was noted among three Groups, but median age of patients was higher in Group 3 (Table 1). Fever was developed in 50% of patients in Group 3 at the initial radiographic change, and in 86% of them during subsequent clinical course, while it was developed in only 11–12% of patients in Group 1 through their clinical course (Table 2). Dyspnea was developed in 57% of patients in Group 3 and in 44% of patients in Group 2 during clinical course, while it was developed in only 14% of patients in Group 1 (Table 2). A total of 88 patients developed fever at the initial change in chest X-ray and/or during subsequent clinical course. Of these, 43 patients received antibiotics, but no radiographical response was obtained in these patients. Five (2%) and seven (2%) patients in Group 1 developed bloody sputum and chest pain, respectively, but none in Group 2 or 3 developed these symptoms. The average interval of chest X-rays taken between the start of radiotherapy and the first appearance of radiographic change was 1.7 weeks for group 1, 1.3 weeks for group 2, and 0.9 weeks for group 3 ($P < 0.001$, Table 3). Interval between the end of radiotherapy and the first change in a chest X-ray was shorter in Group 3 than in Group 2 or Group 1 (Table 3). Of 57 patients in whom the first radiographic change was noted within three weeks, 9 (16%) died of pneumonitis, while radiation-induced lung injury that occurred 10 weeks or later after the end of radiation was easily managed with or without steroid therapy (Table 3). Oxygen content in the blood at the start of steroid therapy was examined in 70 patients of Groups 2 and 3. Oxygen content

Table 1
Patient demographics and radiotherapy performance

Characteristics	Total *N* (%)	Group 1	Group 2	Group 3	*p*-value
		N (%)	*N* (%)	*N* (%)	
Total	385 (100)	307 (80)	64 (17)	14 (4)	
Sex					
Male	300 (78)	240 (78)	47 (73)	13 (93)	0.28
Female	85 (22)	67 (22)	17 (27)	1 (7)	
Age median (range)	65 (28–87)	63 (28–87)	65 (37–83)	71 (65–84)	0.008
Total dose (Gy)					
Median (range)	60 (50–70)	60 (50–70)	60 (50–61)	60 (50–60)	0.50
Intent of radiotherapy					
Curative	298 (77)	232 (76)	52 (81)	14 (100)	0.074
Palliative	87 (23)	75 (24)	12 (19)	0 (0)	
Chemotherapy					
None	121 (31)	101 (33)	15 (23)	5 (36)	0.48
Sequential	121 (31)	93 (30)	25 (39)	3 (21)	
Concurrent	143 (37)	113 (37)	24 (38)	6 (43)	

Table 2
Symptoms through clinical courses

Symptom	At the initial change in chest X-ray				During subsequent clinical course			
	Group 1	Group 2	Group 3	p	Group 1[a]	Group 2[b]	Group3[b]	p
Cough	96 (31)	35 (56)	5 (36)	0.001	85 (28)	38 (59)	5 (36)	<0.001
Sputum	32 (10)	11 (18)	4 (29)	0.049	30 (10)	11 (17)	3 (21)	0.12
Hemosputum	5 (2)	0 (0)	0 (0)	0.53	4 (1)	0 (0)	0 (0)	0.60
Chest pain	7 (2)	0 (0)	0 (0)	0.40	2 (0.6)	0 (0)	0 (0)	0.78
Fever								
None	269 (88)	35 (56)	7 (50)	<0.001	272 (89)	32 (50)	2 (14)	<0.001
37.0–37.9 °C	18 (6)	11 (18)	2 (14)	24 (8)	16 (25)	5 (35)		
38 °C≤	13 (4)	14 (22)	5 (36)	8 (3)	13 (20)	7 (50)		
Not specified	7 (2)	3 (4)	0 (0)	3 (1)	3 (4)	0 (0)		
Dyspnea	43 (14)	14 (22)	6 (43)	0.007	40 (13)	28 (44)	8 (57)	<0.001
Fever or dyspnea	75 (24)	37 (58)	10 (71)	<0.001	65 (21)	49 (77)	14 (100)	<0.001
Any	150 (49)	51 (81)	13 (93)	<0.001	118 (38)	60 (94)	14 (100)	<0.001

[a] During one month period following the initial change in the chest X-ray.
[b] At the start of steroid therapy.

Table 3
The chest X-ray intervals and first radiographic change

Weeks	Group 1	Group 2	Group 3	p-value
The average interval of chest X-rays (weeks)[a]				
Median (range)	1.7 (0.7 to 6.0)	1.3 (0.5 to 4.4)	0.9 (0.5 to 3.8)	<0.001
Duration between the end of radiotherapy and the first radiographic change (weeks)				
Median (range)	9.9 (−2.9 to 45.1)	6.7 (0 to 24.9)	2.4 (0.4 to 10.1)	<0.001
<6	82 (27)	26 (41)	11 (79)	<0.001
6–11.9	116 (38)	29 (45)	3 (21)	
12–17.9	71 (23)	7 (11)	0 (0)	
18≤	38 (12)	2 (3)	0 (0)	

[a] Calculated as follows: the average interval of chest X-rays = (the first radiographic change − the start of radiotherapy)/the number of chest X-rays taken during this period/7).

was slightly decreased (PaO2 = 70–74.9 Torr) in 12 (19%) patients of Group 2 and one (7%) patient of Group 3, and moderately to severely decreased (PaO2 ⩽ 69.9 Torr or SpO2 ⩽ 92%) in 21 (33%) patients of Group 2 and 7 (50%) patients of Group 3 ($p = 0.38$).

Prednisolone was administered as the initial therapy in 69 (88%) patients of Groups 2 and 3. The initial prednisolone equivalent dose of steroid was 30–40 mg daily in 52 (67%), and 60 mg of higher only in 8 (10%) patients (Table 4). The median duration of the initial dose was 10 (range, 2–64) days, and the dose was reduced within 14 days in 57 (77%) patients. The median duration of steroid therapy was 10 (range, 2–28) weeks (Table 4). Steroid pulse therapy (methylprednisolone 1000 mg daily for three days) was administered as the initial therapy in one patient, and as salvage therapy in six patients at the time of pneumonitis aggravation. Among the seven patients, six died of respiratory failure due to progressive radiation pneumonitis.

Outcome of steroid therapy was evaluated in 76 patients (Fig. 1). Symptomatic relief was obtained and the steroid dose was reduced in 71 (93%) of the 76 patients, while no effect was noted in the remaining five patients, who all died of radiation pneumonitis despite escalated steroid administration. Of the 71 patients, 15 (21%) developed recurrent symptoms at the median daily prednisolone dose of 20 mg (range, 10–40 mg) within median 33 days (range, 21–42 days) from the start of the steroid therapy, and required steroids to be escalated. Of the 15 patients, nine died of radiation pneumonitis and one died of complication of steroid therapy. A total of 54 (71%) patients were in remission from pneumonitis and steroid therapy was terminated. The remainder 22 patients died during steroid therapy, 14 of radiation pneumonitis, two of infectious complication (bacterial pneumonia in one, and lung aspergillosis in another patient), five of lung cancer progression, and one of hemoptysis. Thus, 16 patients, who accounted for 4.2% of 385 patients receiving 50–70 Gy of thoracic radiotherapy, and who accounted for 21% of 78 patients treated with steroid therapy, died of radiation pneumonitis or complication associated with steroid therapy. Median survival from the start of steroid therapy in these patients was 45 (range, 8–107) days.

Discussion

Patients with radiation-induced lung injury have been managed in compliance with the expert opinions, because there has been no case series or clinical trial report on clinical course and corticosteroid use for this lung injury. This

Table 4
Corticosteroid, dose and duration of steroid therapy

	N (%)
Corticosteroid	
Prednisolone	69 (88)
Dexamethasone	4 (5)
Betamethasone	4 (5)
Methylprednisolone	1 (1)
Initial dose, mg/body daily (prednisolone equivalent)	
Pulse therapy	1 (1)
60	7 (9)
50	1 (1)
40	10 (13)
30	42 (54)
10–25	17 (22)
Duration of the initial dose, days	
Median (range)	10 (2–64)
⩽14	57 (77)
15–28	9 (12)
29⩽	8 (11)
Not evaluable	4
Total duration of steroid therapy, weeks	
Median (range)	10 (2–28)
⩽6	16 (30)
6.1–12	19 (35)
12.1–18	14 (26)
18.1⩽	5 (9)
Not evaluable	24

study is the first systemic review of these patients both who received corticosteroid therapy and who did not. Comparison between the expert opinions and the results of this study is given below. First, radiation-induced lung injury is severer when a radiographic change appears earlier [5]. In this study, the initial change in a chest X-ray film was observed in 9.9 (range, −3 to 45) weeks in Group 1, in 6.7 (range, 0–25) weeks in Group 2, and 2.4 (range, 0–10) weeks in Group 3 after the end of thoracic radiotherapy. If patients present with symptoms, presumably they receive a chest X-ray. Thus, the patients with symptoms may have radiographic findings seen sooner, since they receive an X-ray when they complain of symptoms. The average interval of chest X-rays taken between the start of radiotherapy and the first appearance of radiographic change was longer in Group 1 than that in groups 2 and 3. The difference, however, was negligibly small when compared with the difference in duration between the end of radiotherapy and the first radiographic change. Second, steroid administration is determined generally based on the severity of symptoms [5]. In this study steroid was used when patients developed dyspnea or fever. Dyspnea has been thought to be the cardinal symptom of radiation pneumonitis but fever to be unusual [5,10]. In this study, however, fever was highly associated with fatal radiation pneumonitis; fever was noted in 12% patients of Group 1, in 58% patients of Group 2, and 86% patients of Group 3. This study failed to show utility of blood gas analysis. An oxygen content in the blood was decreased moderately to severely in only 28 (36%) patients in Groups 2 and 3, and did not differ between the two groups. The oxygen content in Group 1 was measured in only small number of patients, and therefore it was not evaluable in this study. Third, 30–100 mg/day of prednisolone has been recommended as the initial dose [4–6,10]. In our practice, a dose of 30–40 mg was the most frequently used. We selected this relatively low dose of steroid mostly because steroid therapy was started in out patient clinic. Forth, duration of the initial dose was within two weeks in 73% of patients, which is consistent to most expert opinions [6,10]. In contrast, tapering schedules varied between a pa-

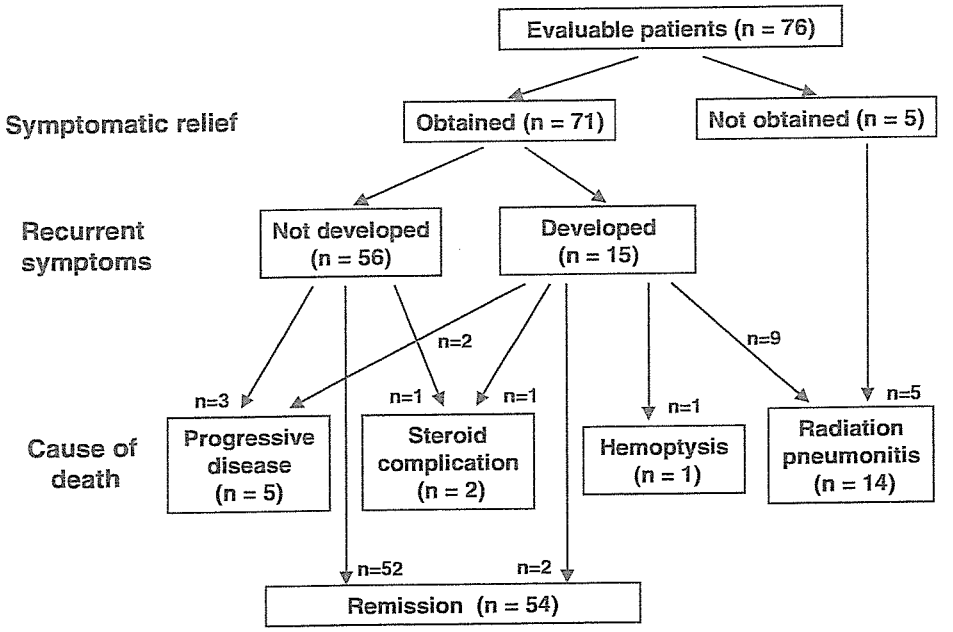

Fig. 1. Outcome of patients who received steroid therapy. Two patients were excluded because of loss of follow-up. Of 76 evaluable patients, 71 (93%) experienced symptomatic relief by steroid therapy.

tient and another in this study. This may be partly due to the diversity in clinical course of radiation pneumonitis, but mostly due to lacking in available recommendation for tapering schedules. In this study, median total duration of steroid therapy was 10 weeks, which may be a tentative guide. A guideline of taper schedule appeared in the latest textbook: the dose should be tapered by 10 mg every two weeks, and be terminated in 12 weeks [10].

Although our clinical practice mostly followed the expert opinions on the management of radiation-induced lung injury as mentioned above, there is little evidence that our steroid use, dose and duration for radiation-induced lung injury were correct. In this study, 21% of patients received steroid therapy and 4% of patients died of radiation pneumonitis among lung cancer patients treated with thoracic radiotherapy at a total dose of 50 Gy or higher. These figures are comparable to the incidence of grade 3 pneumonitis, 3–20%, and that of fatal pneumonitis, 1–4%, in other reports [10].

In conclusion, development of fever and dyspnea, and short interval between the end of radiotherapy and the first radiographic change were associated with fatal radiation-induced lung injury. Prednisolone 30–40 mg daily for two weeks followed by slow taper was selected for the treatment in many patients.

Acknowledgements

This work was supported in part by Grants-in-Aid for Cancer Research from the Ministry of Health, Labour and Welfare of Japan. We thank Yuko Yabe and Mika Nagai for preparation of the manuscript.

* **Corresponding author**: **Ikuo Sekine**, Division of Internal Medicine and Thoracic Oncology, National Cancer Center Hospital, Tsukiji 5-1-1, Chuo-ku, Tokyo 104-0045, Japan. *E-mail address:* isekine@ncc.go.jp

Received 11 October 2005; received in revised form 19 April 2006; accepted 23 May 2006; Available online 3 July 2006

References

[1] Groover TA, Christie AC, Merritt EA. Observations on the use of the copper filter in the roentgen treatment of deep-seated malignancies. South Med J 1922;15:440–4.
[2] Hines LE. Fibrosis of the lung following roentgen-ray treatments for tumor. JAMA 1922;79:720–2.
[3] Evans WA, Leucutia T. Intrathoracic changes induced by heavy radiation. Am J Roentgenol 1925;13:203–20.
[4] Gross NJ. Pulmonary effects of radiation therapy. Ann Intern Med 1977;86:81–92.
[5] Stover D, Kaner R. Pulmonary toxicity. In: DeVita Jr V, Hellman S, Rosenberg S, editors. Cancer: principles and practice of oncology. Philadelphia: Lippincott Williams & Wilkins; 2001. p. 2894–904.
[6] McDonald S, Rubin P, Phillips TL, Marks LB. Injury to the lung from cancer therapy: clinical syndromes, measurable endpoints, and potential scoring systems. Int J Radiat Oncol Biol Phys 1995;31:1187–203.
[7] Inoue A, Kunitoh H, Sekine I, et al. Radiation pneumonitis in lung cancer patients: a retrospective study of risk factors and the long-term prognosis. Int J Radiat Oncol Biol Phys 2001;49:649–55.
[8] Cosgriff SW, Kligerman MM. Use of ACTH and cortisone in the treatment of post-irradiation pulmonary reaction. Radiology 1951;57:536–40.
[9] Rubin P, Casarett GW. Clinical Radiation Pathology. Philadelphia: WB Saunders Co; 1968.
[10] Machtay M. Pulmonary complications of anticancer treatment. In: Abeloff M, Armitage JO, Niederhuber JE, Kastan MB, McKenna WG, editors. Clin. Oncol.. Philadelphia: Elsevier Churchill Livingstone; 2004. p. 1237–50.
[11] Pezner RD, Bertrand M, Cecchi GR, et al. Steroid-withdrawal radiation pneumonitis in cancer patients. Chest 1984;85:816–7.
[12] Parris TM, Knight JG, Hess CE, Constable WC. Severe radiation pneumonitis precipitated by withdrawal of corticosteroids: a diagnostic and therapeutic dilemma. Am J Roentgenol 1979;132:284–6.
[13] Castellino RA, Glatstein E, Turbow MM, et al. Latent radiation injury of lungs or heart activated by steroid withdrawal. Ann Intern Med 1974;80:593–9.

Docetaxel Consolidation Therapy Following Cisplatin, Vinorelbine, and Concurrent Thoracic Radiotherapy in Patients with Unresectable Stage III Non-small Cell Lung Cancer

Ikuo Sekine, Hiroshi Nokihara,* Minako Sumi,† Nagahiro Saijo,‡ Yutaka Nishiwaki,§ Satoshi Ishikura,|| Kiyoshi Mori,¶ Iwao Tsukiyama,# and Tomohide Tamura**

Background: To evaluate the feasibility and efficacy of docetaxel consolidation therapy after concurrent chemoradiotherapy for unresectable stage III non–small cell lung cancer (NSCLC).

Patients and Methods: The eligibility criteria included unresectable stage III NSCLC, no previous treatment, age between 20 and 74 years, and performance status 0 or 1. Treatment consisted of cisplatin (80 mg/m^2 on days 1, 29, and 57), vinorelbine (20 mg/m^2 on days 1, 8, 29, 36, 57, and 64), and thoracic radiotherapy (TRT) (60 Gy/30 fractions over 6 weeks starting on day 2), followed by consolidation docetaxel (60 mg/m^2 every 3 to 4 weeks for three cycles).

Results: Of 97 patients who were enrolled in this study between 2001 and 2003, 93 (76 males and 17 females with a median age of 60) could be evaluated. Chemoradiotherapy was well tolerated; three cycles of chemotherapy and 60 Gy of TRT were administered in 80 (86%) and 87 (94%) patients, respectively. Grade 3 or 4 neutropenia, esophagitis, and pneumonitis developed in 62, 11, and 3 patients, respectively. Docetaxel consolidation was administered in 59 (63%) patients, but three cycles were completed in only 34 (37%) patients. The most common reason for discontinuation was pneumonitis, which developed in 14 (24%) of the 59 patients. During consolidation therapy, grade 3 or 4 neutropenia, esophagitis, and pneumonitis developed in 51, 2, and 4 patients, respectively. A total of four patients died of pneumonitis. We calculated a V_{20} (the percent volume of the normal lung receiving 20 Gy or more) on a dose–volume histogram in 25 patients. Of these, five patients developed grade 3 or more severe radiation pneumonitis. A median V_{20} for these five patients was 35% (range, 26–40%), whereas the median V_{20} for the remaining 20 patients was 30% (range, 17–35%) (p = 0.035 by a Mann–Whitney test). The response rate was 81.7% (95% confidence interval [CI], 72.7–88.0%), with 5 complete and 71 partial responses. The median progression-free survival was 12.8 (CI, 10.2–15.4) months, and median survival was 30.4 (CI, 24.5–36.3) months. The 1-, 2-, and 3-year survival rates were 80.7, 60.2, and 42.6%, respectively.

Conclusion: This regimen produced promising overall survival in patients with stage III NSCLC, but the vast majority of patients could not continue with the docetaxel consolidation because of toxicity.

Key Words: Non-small cell lung cancer, Chemoradiotherapy, Consolidation, Docetaxel.

(*J Thorac Oncol.* 2006;1: 810–815)

Locally advanced unresectable non–small cell lung cancer (NSCLC), stage IIIA with bulky N2 and stage IIIB disease without pleural effusion, is characterized by large primary lesions and/or involvement of the mediastinal or supraclavicular lymph nodes and occult systemic micrometastases. A combination of thoracic radiotherapy and chemotherapy is the standard medical treatment for this disease, but the optimal combination has not been established.[1] Although the available data are insufficient to accurately define the size of a potential benefit,[2] concurrent chemoradiotherapy using a platinum doublet has been shown to be superior to the sequential approach in phase III trials of this disease.[3–5] However, third-generation cytotoxic agents, which have provided better patient survival with extrathoracic spread than the old-generation agents, must be reduced when administered concurrently with thoracic radiotherapy.[6] Thus, it has been hypothesized that the addition of systemic dose chemotherapy with a new cytotoxic agent to concurrent chemoradiotherapy, either as induction or as consolidation chemotherapy, might further improve patient survival.[1]

The consolidation chemotherapy with docetaxel was based on the observation that this drug was highly active in the primary treatment of metastatic NSCLC, producing a response rate (RR) as high as 20% after platinum-based chemotherapy failed.[7–9] Highly encouraging results of a me-

Divisions of *Internal Medicine and Thoracic Oncology, and †Radiation Oncology, National Cancer Center Hospital, Tokyo, Japan; Divisions of ‡Internal Medicine, §Thoracic Oncology, and ||Radiation Oncology, National Cancer Center Hospital East, Kashiwa, Japan; and Divisions of ¶Thoracic Oncology and #Radiotherapy, Tochigi Cancer Center, Utsunomiya, Japan.

Address for correspondence: Ikuo Sekine, Division of Thoracic Oncology and Internal Medicine, National Cancer Center Hospital, Tsukiji 5-1-1, Chuo-ku, Tokyo 104-0045, Japan. E-mail: isekine@ncc.go.jp

ISSN: 1556-0864/06/0108-0810

dian survival time (MST) of more than 2 years and a 3-year survival rate of nearly 40% were obtained in a phase II trial of docetaxel consolidation after chemoradiotherapy with cisplatin and etoposide in patients with stage IIIB NSCLC (SWOG study S9504).[10]

We have developed a combination chemotherapy schedule with cisplatin and vinorelbine concurrently administered with thoracic radiotherapy at a total dose of 60 Gy in 30 fractions in patients with unresectable stage III NSCLC. The results of a phase I study in 18 patients were very promising, with a RR of 83%, a MST of 30 months, and a 3-year survival rate of 50%.[6] Thus, addition of docetaxel consolidation to this regimen is a particularly interesting therapeutic strategy. The objectives of the current study were to evaluate the feasibility of docetaxel consolidation therapy after concurrent chemoradiotherapy with cisplatin and vinorelbine and to evaluate the efficacy and safety of the whole treatment regimen including both the chemoradiotherapy and consolidation therapy in patients with unresectable stage IIIA and IIIB NSCLC.

PATIENTS AND METHODS

Patient Selection

The eligibility criteria were histologically or cytologically proven NSCLC; unresectable stage IIIA or IIIB disease; no previous treatment; measurable disease; tumor within an estimated irradiation field no larger than half the hemithorax; age between 20 and 74 years; Eastern Cooperative Oncology Group performance status (PS) of 0 or 1; adequate bone marrow function (12.0×10^9/liter ≥ white blood cell [WBC] count ≥4.0×10^9/liter, neutrophil count ≥2.0×10^9/liter, hemoglobin ≥10.0 g/dl, and platelet count ≥100×10^9/liter), liver function (total bilirubin ≤1.5 mg/dl and transaminase no more than twice the upper limit of the normal value), and renal function (serum creatinine ≤1.5 mg/dl and creatinine clearance ≥60 ml per minute); and a PaO_2 of 70 torr or more under room air conditions. Patients were excluded if they had malignant pleural or pericardial effusion, active double cancer, a concomitant serious illness such as uncontrolled angina pectoris, myocardial infarction in the previous 3 months, heart failure, uncontrolled diabetes mellitus, uncontrolled hypertension, interstitial pneumonia or lung fibrosis identified by a chest x-ray, chronic obstructive lung disease, infection or other diseases contraindicating chemotherapy or radiotherapy, pregnancy, or if they were breast feeding. All patients gave their written informed consent.

Pretreatment Evaluation

The pretreatment assessment included a complete blood cell count and differential count, routine chemistry determinations, creatinine clearance, blood gas analysis, electrocardiogram, lung function testing, chest x-rays, chest computed tomographic (CT) scan, brain CT scan or magnetic resonance imaging, abdominal CT scan or ultrasonography, and radionuclide bone scan.

Treatment Schedule

Treatment consisted of a chemoradiotherapy phase with three cycles of cisplatin and vinorelbine followed by a consolidation phase with three cycles of docetaxel (Figure 1). Cisplatin 80 mg/m^2 was administered on days 1, 29, and 57 by intravenous infusion for 60 minutes with 2500 to 3000 ml of fluid for hydration. Vinorelbine diluted in 50 ml of normal saline was administered intravenously on days 1, 8, 29, 36, 57, and 64. All patients received prophylactic antiemetic therapy consisting of a $5HT_3$-antagonist and a steroid.

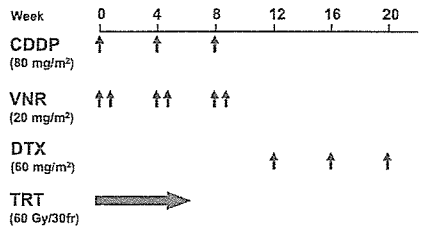

FIGURE 1. Treatment schema. CDDP, cisplatin; DTX, docetaxel; TRT, thoracic radiotherapy; VNR, vinorelbine.

Radiation therapy was delivered with megavoltage equipment (≥6 MV) using anterior/posterior opposed fields up to 40 Gy in 20 fractions including the primary tumor, the metastatic lymph nodes, and the regional nodes. A booster dose of 20 Gy in 10 fractions was given to the primary tumor and the metastatic lymph nodes for a total dose of 60 Gy using bilateral oblique fields. A CT scan–based treatment planning was used in all patients. The clinical target volume (CTV) for the primary tumor was defined as the gross tumor volume (GTV) plus 1 cm taking account of subclinical extension. CTV and GTV for the metastatic nodes (>1 cm in shortest dimension) were the same. Regional nodes, excluding the contralateral hilar and supraclavicular nodes, were included in the CTV, but the lower mediastinal nodes were included only if the primary tumor was located in the lower lobe of the lung. The planning target volumes for the primary tumor, the metastatic lymph nodes, and regional nodes were determined as CTVs plus 0.5- to 1.0-cm margins laterally and 1.0- to 2.0-cm margins craniocaudally, taking account of setup variations and internal organ motion. Lung heterogeneity corrections were not used.

The criteria for starting consolidation chemotherapy were completion of three cycles of cisplatin and vinorelbine and a full dose of thoracic radiotherapy, the absence of progressive disease, adequate general condition within 6 weeks of the start of the third cycle of cisplatin and vinorelbine (PS 0 or 1, WBC count ≥3.0×10^9/liter, neutrophil count ≥1.5×10^9/liter, hemoglobin ≥9.0 g/dl and platelet count ≥100×10^9/liter, total bilirubin ≤1.5 mg/dl and transaminase no more than twice the upper limit of the normal value, and a PaO_2 of 70 torr or more at room air). Docetaxel (60 mg/m^2) was administered intravenously for 1 hour every 3 to 4 weeks for three cycles.

Toxicity Assessment and Treatment Modification

Complete blood cell counts and differential counts, routine chemistry determinations, and a chest x-ray were performed once a week during the course of treatment. Acute toxicity was graded according to the NCI Common Toxicity Criteria, and late toxicity associated with thoracic radiother-

apy was graded according to the Radiation Therapy Oncology Group/European Organization for Research and Treatment of Cancer late radiation morbidity scoring scheme. Vinorelbine administration on day 8 was omitted if any of the following were noted: WBC count $<3.0 \times 10^9$/liter, neutrophil count $<1.5 \times 10^9$/liter, platelet count $<100 \times 10^9$/liter, elevated hepatic transaminase level or total serum bilirubin of at least grade 2, fever ≥38°C, or PS ≥2. Subsequent cycles of cisplatin and vinorelbine chemotherapy were delayed if any of the following toxicities were noted on day 1: WBC count $<3.0 \times 10^9$/liter, neutrophil count $<1.5 \times 10^9$/liter, platelet count $<100 \times 10^9$/liter, serum creatinine level ≥1.6 mg/dl, elevated hepatic transaminase level or total serum bilirubin of at least grade 2, fever ≥38°C, or PS ≥2. The dose of cisplatin was reduced by 25% in all subsequent cycles if the serum creatinine level rose to 2.0 mg/dl or higher. The dose of vinorelbine or docetaxel was reduced by 25% in all subsequent cycles if any of the following toxicities were noted: WBC count $<1.0 \times 10^9$/liter, platelet count $<10 \times 10^9$/liter, or grade 3 or 4 infection or liver dysfunction. Thoracic radiotherapy was suspended if any of the following were noted: fever ≥38°C, grade 3 esophagitis, PS of 3, or PaO_2 <70 torr. Thoracic radiotherapy was terminated if any of the following were noted: grade 4 esophagitis, grade 3 or 4 pneumonitis, PS of 4, or duration of radiotherapy of over 60 days. The use of granulocyte colony-stimulating factor during radiotherapy was not permitted unless radiotherapy was on hold. The criteria for termination of docetaxel consolidation were not defined in the protocol.

Response Evaluation

Objective tumor response was evaluated according to the Response Evaluation Criteria in Solid Tumor.[11] Local recurrence was defined as tumor progression in the primary site and in the hilar, mediastinal, and supraclavicular lymph nodes after a partial or complete response; regional recurrence as the development of malignant pleural and pericardial effusions; and distant recurrence as the appearance of a distant metastasis.

Study Design, Data Management, and Statistical Considerations

This study was conducted at three institutions: the National Cancer Center Hospital, National Cancer Center Hospital East, and Tochigi Cancer Center. The protocol and consent form were approved by the institutional review board of each institution. Registration was conducted at the registration center. Data management, periodic monitoring, and the final analysis were performed by the study coordinator.

The primary objective of the current study was to evaluate the feasibility of docetaxel consolidation therapy. The secondary endpoints were toxicity observed during chemoradiotherapy and consolidation therapy, the best response, and overall survival in all patients eligible to participate in this study. Because no standard method to evaluate consolidation chemotherapy after chemoradiotherapy has been established, we arbitrarily defined the primary endpoint of this study as a ratio (R) of the number of patients receiving docetaxel without grade 4 nonhematological toxicity or treatment-related death to the total number of patients receiving docetaxel. The sample size was initially estimated to be 34 patients with a power of 0.80 at a significance level of 0.05, under the assumption that a R of 0.95 would indicate potential usefulness, whereas a R of 0.8 would be the lower limit of interest, and that 85% of patients would move into the consolidation phase. An analysis of the first 13 patients, however, showed that only 8 (61%) patients advanced into the consolidation phase. The reasons for not receiving docetaxel were disease progression in one, delay in completion of chemoradiotherapy in two, grade 3 esophagitis in one, and death due to hemoptysis in one patient. Considering that the SWOG trial S9504 included 83 patients, we decided to revise the number of patients in the current study. According to Simon's two-stage minimax design, the required number of patients was calculated to be 59 with a power of 0.80 at a significance level of 0.05, under the assumption that a R of 0.85 would indicate potential usefulness, whereas a R of 0.7 would be the lower limit of interest.[12] Assuming that 61% of registered patients would move into the consolidation phase, the sample size was determined to be 97 patients.

Overall survival time and progression-free survival time were estimated by the Kaplan–Meier method, and confidence intervals (CI) were based on Greenwood's formula.[13] Overall survival time was measured from the date of registration to the date of death (from any cause) or to the last follow-up. Progression-free survival time was measured from the date of registration to the date of disease progression, death (from any cause), or the last follow-up. Patients who were lost to follow-up without event were censored at the date of their last known follow-up. A CI for RR was calculated using methods for exact binomial CIs. The Dr. SPSS II 11.0 for Windows software package (SPSS Japan Inc., Tokyo, Japan) was used for statistical analyses.

RESULTS

Registration and Characteristics of the Patients

A total of 97 patients were enrolled in this study between April 2001 and June 2003. Four patients were excluded from this study before the treatment was started because the radiation treatment planning disclosed that their tumors were too advanced for curative thoracic radiotherapy. Thus, 93 patients who received the protocol-defined treatment were the subjects of this analysis (Figure 2). There were 76 males and 17 females, with a median age of 60 (range 31–74). Body weight loss was less than 5% in 77 patients; adenocarcinoma histology was noted in 57 patients, and stage IIIA disease was noted in 41 patients (Table 1).

Treatment Delivery

Treatment delivery was generally well maintained in the chemoradiotherapy phase (Table 2). Full cycles of cisplatin and vinorelbine and the full dose of thoracic radiotherapy were administered in 80 (86%) and 87 (94%) patients, respectively. Delay in radiotherapy was less than 5 days in 61 (66%) patients. In contrast, the delivery of docetaxel was poor (Table 2). A total of 59 (63%) patients could enter the consolidation phase, and only 34 (37%) patients completed three cycles of docetaxel chemotherapy. The reasons for not

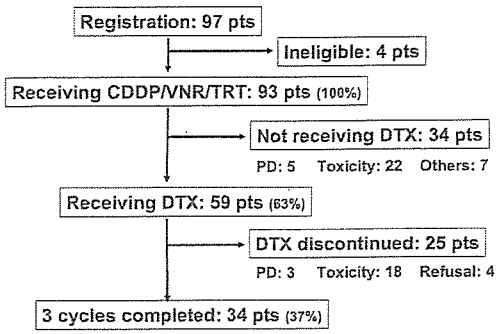

FIGURE 2. Patient registration. CDDP, cisplatin; DTX, docetaxel; TRT, thoracic radiotherapy; VNR, vinorelbine.

receiving consolidation were toxicity in 22 (65%) patients including pneumonitis in seven patients, myelosuppression in five patients, esophagitis in four patients, liver dysfunction in two patients, infection in two patients, other toxicity in two patients, progressive disease in five (15%) patients, patient refusal in three (9%) patients, early death due to hemoptysis in one (3%) patient, and other reasons in three (9%) patients. Of the 59 patients, 18 (31%) discontinued docetaxel consolidation because of toxicity, including pneumonitis (n = 14) and esophagitis, infection, gastric ulcer, and allergic reaction (n = 1 each), four (7%) because of patient refusal, and three (5%) because of progressive disease.

Toxicity

Acute severe toxicity in the chemoradiotherapy phase was mainly leukopenia and neutropenia, whereas grade 3 or 4 thrombocytopenia was not noted (Table 3). Severe nonhematological toxicity was sporadic, and grade 3 esophagitis and pneumonitis were observed in only 11 (12%) and 3 (3%) patients, respectively. Acute severe toxicity in the consolidation phase also consisted of neutropenia and associated infection (Table 4). In addition, grade 3 or 4 pneumonitis developed in 4 (7%) patients. The R observed in this study was 0.05 (3 out of 57 patients), which was much lower than the hypothetical value. Grade 3 or 4 late toxicities were included lung toxicity in four patients, esophageal toxicity in two patients, renal toxicity in one patient, and a second esophageal cancer that developed 35.4 months after the start of the chemoradiotherapy in one patient. Treatment-related

TABLE 1. Patient Characteristics

Characteristics	n	%
Gender		
Male	76	82
Female	17	18
Age median (range)	60	31–74
Weight loss		
<5%	76	81
5–9%	12	13
≥10%	3	3
Unknown	2	2
Histology		
Adenocarcinoma	57	61
Squamous cell carcinoma	23	25
Large cell carcinoma	12	13
Others	1	1
Stage		
IIIA	41	44
IIIB	52	56

TABLE 2. Treatment Delivery

Variables	n	%
Cisplatin and vinorelbine chemotherapy		
Total number of cycles		
3	80	86
2	10	11
1	3	3
Number of vinorelbine skips		
0	63	68
1	25	27
2–3	5	5
Thoracic radiotherapy		
Total dose (Gy)		
60	87	94
50–59	4	4
<50	2	2
Delay (days)		
<5	61	66
5–9	20	22
10–16	6	6
Not evaluable (<60 Gy)	6	6
Docetaxel consolidation		
Number of cycles		
3	34	37
2	12	13
1	13	14
0	34	34

TABLE 3. Acute Toxicity in Chemoradiotherapy (n = 93)

	Grade			
Toxicity	3	4	3 + 4	%
Leukopenia	54	18	72	77
Neutropenia	33	29	62	67
Anemia	21	0	21	23
Infection	15	1	16	17
Esophagitis	11	0	11	12
Hyponatremia	11	0	11	12
Anorexia	9	1	10	11
Nausea	5	—	5	5
Pneumonitis	3	0	3	3
Syncope	2	0	2	2
Hyperkalemia	2	0	2	2
Ileus	0	1	1	1
Cardiac ischemia	1	0	1	1